TECHNISCHE UNIVERSITÄT WIEN
Vienna University of Technology

DIPLOMARBEIT

Further development of the software jGiXa for Grazing incidence X-ray fluorescence analysis

ausgeführt am
Atominstitut
der Technischen Universität Wien
Stadionallee 2
1020 Wien

unter der Anleitung von
Ao.Univ.Prof. Dipl.-Ing. Dr.techn. Christina Streli
und
Univ. Ass. Dipl.-Ing. Dr.techn. Dieter Ingerle

durch
Michael Iro
Theresianumgasse 13/1/9
1040 Wien

Unterschrift Student

Unterschrift Betreuerin

Wien, am 8. Mai 2019

Abstract

Combined Grazing incidence X-Ray fluorescence and X-Ray reflectometry analysis, as proposed by de Boer [1], needs a sophisticated software using global optimization algorithms to fit calculated curves for a specific sample-setup-model to measurement results of angle dependent fluorescence signals from ultra thin layers on a reflecting surface (e.g. Si-wafer). The software package jGiXa, developed by Ingerle [2] for this purpose, used a graphical user interface and optimization algorithms based on MatLab code and a Java based calculation of the spectra.

This diploma thesis focuses on the further development of the jGiXa software. Therefor a Java based graphical user interface and global optimization algorithm were implemented, allowing jGiXa to work as a Java standalone software. This is advantageous in respect to portability, usability, maintainability, scalability, performance, etc. To further optimize the performance of the software a meta optimization was implemented to find ideal parameters for the global optimization algorithm. Furthermore a new model for intermediate layers was implemented, to allow sample models with a continuous transition between layers. To test the new software, comparison evaluations for different measurements were made.

Zusammenfassung

Kombinierte Röntgenfluoreszenzanalyse unter streifendem Einfall und Röntgenreflektometrie, wie von de Boer [1] vorgeschlagen, benötigt eine elaborierte Software, welche globale Optimierungsalgorithmen nutzt um berechnete Kurven eines spezifischen Probe-Setup-Modells an Messdaten von winkelabhängigen Fluoreszenzsignalen ultra-dünner Schichten auf reflektierenden Oberflächen (z.B. Si-Wafer) anzupassen. Das Softwarepaket jGiXa, welches von Ingerle [2] zu diesem Zweck entwickelt wurde, verwendet eine grafische Benutzeroberfläche und Optiemirungsalgorithmen basierend auf MatLab code und eine Java basierte Berechnung der Spektren.

Diese Diplomarbeit beschäftig sich mit der Weiterentwicklung der jGiXa software. Dafür wurden eine Java basierte graphische Benutzeroberfläche und ein globaler Optimierungsalgorithmus implementiert um jGiXa als Java standalone software betreiben zu können. Dies bietet zahlreich Vorteile in Hinsicht auf Portabilität, Benutzerfreundlichkeit, Wartbarkeit, Erweiterbarkeit, Leistung etc.. Um die Leistung der Software weiter zu optimieren wurde eine Meta-Optimierung implementiert um ideale Parameter für den globalen Optimierungsalgorithmus zu finden. Weiters wurde ein Modell von Zwischenschichten implementiert, um die Beschreibung von Probemodellen mit kontinuierlichen Übergängen zwischen Schichten zu beschreiben. Zum Test der neuen Software wurden Vergleichsberechnungen verschiedener Messungen durchgeführt.

Acknowledgements

I would like to thank Dr. Christina Streli, Dr. Dieter Ingerle and Dr. Peter Wobrauschek for their excellent supervision of my work for project and master thesis. Also I want to thank all other members of the X-ray-physics group at the Atominstitut of the TU Wien for their support and for the good working atmosphere in the group.

Representative for all of the colleagues and friends who supported me and helped making my time at university a productive and enjoyable time I want to thank some people in particular: Felix Linhardt for his support in the first semesters, Andrea Tröstl for hours of help learning and encouragement in times of need and Paul Häuslmayer and Christoph Mehofer, for their help proofreading my project thesis.

Contents

1 Introduction

The non-destructive investigation of ultra-thin layers gains importance as the thickness of semiconductor layers decrease. In the 1990s de Boer and Van Den Hoogenhof published a series of papers [1, 6, 5, 4, 3] discussing possible combinations of X-ray analytical methods, for a setup where the primary radiation hits the sample under an angle of incidence around the critical angle, naming this combination Glancing incidence X-ray analysis (GIXA). These combined measurements allow a precise investigation of ultra-thin layers and their composition-depth profile.

At the Atominstitut of the TU Wien, in the the 2010s Ingerle [7, 2] build a setup for a tabletop spectrometer for combined Grazing incidence X-ray fluorescence analysis (GIXRF) and X-ray reflectometry (XRR) as proposed by de Boer and Van Den Hoogenhof, and started the jGiXa project to evaluate these GIXA measurements. Exploiting the powerful global optimization packages implemented in MatLab and the easy to use parallelization methods of Java, jGiXa 1.0 comprised of a graphical user interface and global optimization algorithms based on MatLab code and a Java based calculation of the fluorescence and reflected X-ray intensities. Over time it became clear that this separation, would become hard to maintain, as Java and MatLab develop as does jGiXa itself.

This diploma thesis focuses on the further development of the software jGiXa. To allow jGiXa to work as a Java standalone software a graphical user interface and a global optimization algorithm were implemented. As a global optimization algorithm, the differential evolution algorithm [8] developed by Price and Storn, was chosen adapting the code from [9]. The graphical user interface was built, using the MVC design pattern [10]. The result being a Java standalone software that, poses many advantages, compared to the old software, concerning usability, maintainability and performance, but most of all allows further development of the software to be more easily partible, i.e. making it possible to be done by project students without a long time getting to know all parts of the code.

Further a new model for roughness was implemented. Other than the previous model for roughness as a single parameter of a layer, the new approach allows continuous transitions between layers, by adding intermediate layers with continuous transition functions for density and material composition.

The differential evolution algorithm [8] itself has many parameters. Different combinations of those parameters have varying prospects of success for different applications. To investigate a possible ideal parameter setup for jGiXa in general or samples with a similar sample model in particular a meta-optimization was implemented, brute-forcing through many parameter combinations for the algorithm. This could be done in a reasonable time, due to the vast improvement of speed, by the work for this master thesis.

To test the accuracy and performance of the new software measurements taken with two different setups were evaluated. A 50 nm Ni sample, measured both at the X-ray Center (XRC) of the TU Wien and the Atominstitut of the TU Wien and a 10nm Ti sample measured at the XRC were evaluated, comparing the results and performance of jGiXa 2.0 with its predecessor.

2 A short Introduction to Glancing Incidence X-ray analysis (GIXA)

Since the discovery of X-rays by Wilhelm Conrad Röntgen in 1895, X-rays have found a wide array of applications in medicine, material science, and various other scientific fields. This diploma thesis discusses the further development of a software package for the evaluation of combined GIXRF and XRR measurements. For readers without prior knowledge in X-ray analytics, some basic principles are explained in the following section. The explanation focuses on the production of X-rays with X-ray tubes, monochromatization with multilayers and crystals and detection with silicon drift detectors (SDD), to match the setups at the Atominstitut (ATI) of the TU Wien (see section 4.1.2) and the X-ray-Center (XRC) of the TU Wien (see section 4.1.1) and therefore neglects different methods of X-ray production, monochromatization and detection. Nevertheless the jGiXa software can be applied to different setups since the mathematical model is only dependent of a few simple parameters for the setup (see section 4). A more detailed introduction to X-ray analytics can be found in [11].

2.1 Production and monochromatization of X-rays

X-rays, can be produced with an X-ray tube (see figure 1) accelerating electrons from a cathode to an anode, where they are decelerated by the electromagnetic field of the atoms of the anode material, emitting continuous radiation. Some of the electrons ionize atoms of the anode material, thereby producing characteristic radiation.

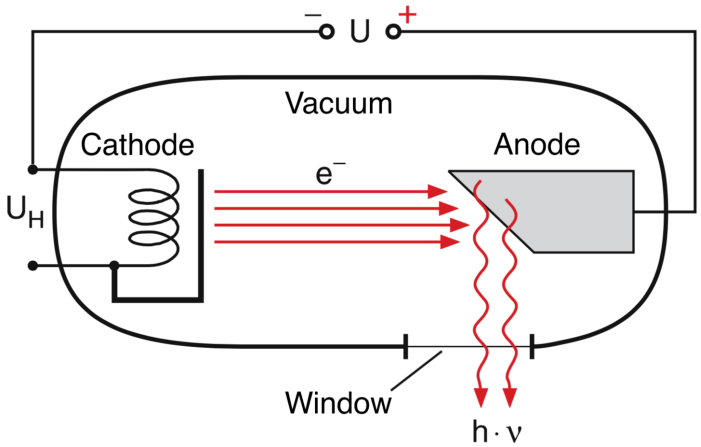

Figure 1: Working principle of an X-ray tube from [12]

2.1.1 Continuous radiation

Accelerated charged particles emit electromagnetic radiation [12]. In an X-ray tube, electrons are deflected by the electromagnetic field of the atomic nuclei of the anode material. The energy of the emitted radiation is a result of the energy balance of the deflection

$$E_r = E_b - E_a \tag{1}$$

with E_r being the energy of the emitted electromagnetic radiation, E_b being the energy of the electron before the acceleration and E_a being the energy of the electron after the acceleration. This process is shown in figure 2.

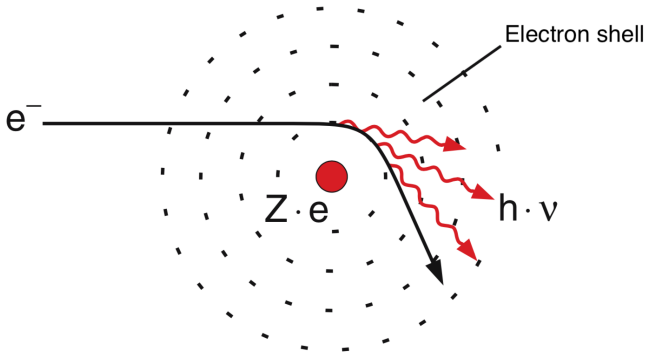

Figure 2: Creation of continuous radiation from [12]

2.1.2 Characteristic radiation

When an atom is ionized, through ejection of an electron from an inner shell, electrons from higher energy states can fill the void left by this ionization emitting radiation. The energy of this radiation is a result of the energy balance of the transition process:

$$E_r = E_h - E_l \tag{2}$$

with E_r being the energy of the emitted electromagnetic radiation, E_h being the energy of the electron in the higher energy state and E_l being the energy of the electron in the lower energy state. This radiation is called characteristic radiation because its energy is characteristic for a specific transition of a specific element. In case of the X-ray tube the emitted radiation is characteristic for transitions of the anode material and the initial ionization is a result of an interaction of accelerated electrons with the atoms of the anode material. The effect of

characteristic radiation will also be of importance for XRF (see section 2.3) where the initial ionization is a result of an interaction of X-rays with the sample material and the emitted radiation is characteristic for the sample material. Figure 3 shows the possible transitions.

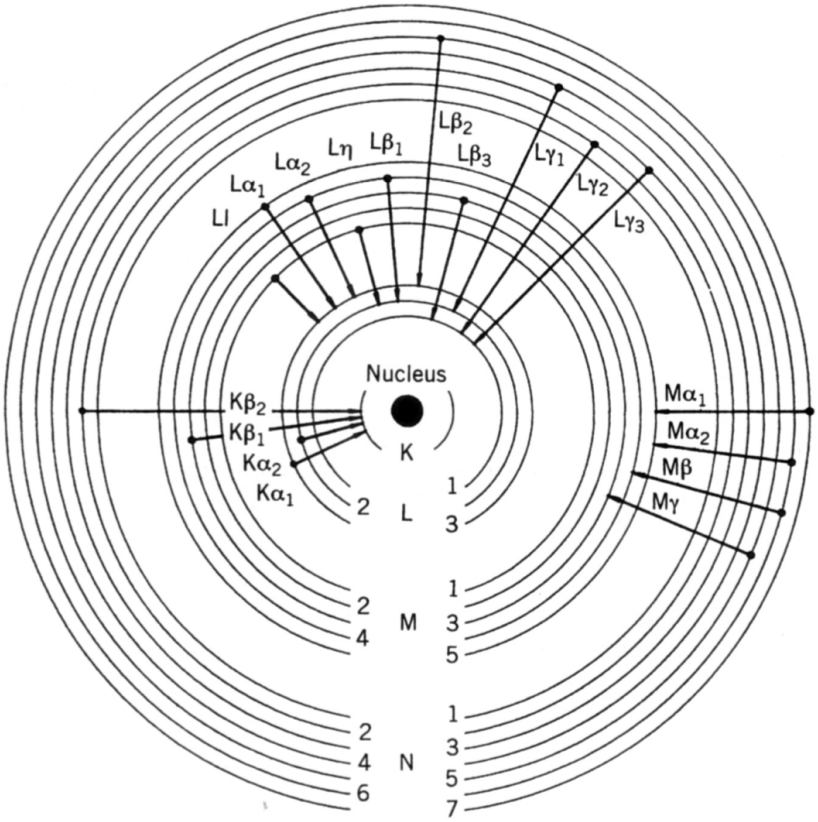

Figure 3: Possible transitions for characteristic radiation in Siegbahn notation from [13]

These two effects lead to a continuous energy spectrum with characteristic peaks, which can be seen in figure 4.

2.1.3 Monochromatization

Because of the energy-dependence of the refractive index of matter (see section 2.3.2), it is necassary for Grazing Incidence X-ray fluorescence analysis (GIXRF) to use a nearly monochrome primary radiation. Both multilayer and crystal monochromators, utilize Bragg's law (see figure 5), which describes the condition for positive interference of electromagnetic

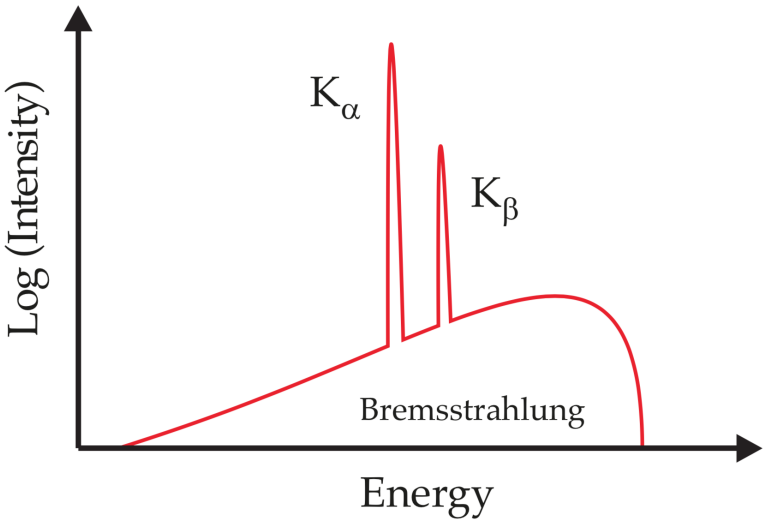

Figure 4: Continuous X-ray spectrum with characteristic peaks from [14]

radiation in matter:

$$2 \cdot d \cdot sin(\alpha) \approx n \cdot \lambda \tag{3}$$

with d being the distance between neighboring planes of reflection, α being the angle of incidence, n being an integer number and λ being the wavelength of the incoming radiation. Only the waves, with a phase difference $\Delta\phi = 0$ interfere constructively. This is only the case if the path difference $2 \cdot d \cdot sin(\alpha)$ equals an integer of λ. Figure 5 depicts Bragg's law for atoms of a crystal structure.

A multilayer monochromator is a repeated succession of two layers of materials with constant thicknesses d_1 and d_2 and different refraction indices n_1 and n_2. An incoming plane wave with a wide spectrum of energies, hitting the multilayer, will be partly refracted and partly reflected, at each transition surface. While most energies will be prone to destructive interference, a small energy bandwidth, where the path difference of the radiation is an integer of the wavelength λ, interferes constructively. Figure 6 shows a schematic drawing of the working principle of a multilayer monochromator.

Both kinds of monochromators can therefore be applied to use only a small bandwidth out of an incoming plane wave with a wide spectrum of energies, by choosing the correct angle of incidence. Some hybrid monochromators use a combination of multilayers and crystals (see section 4.1.1).

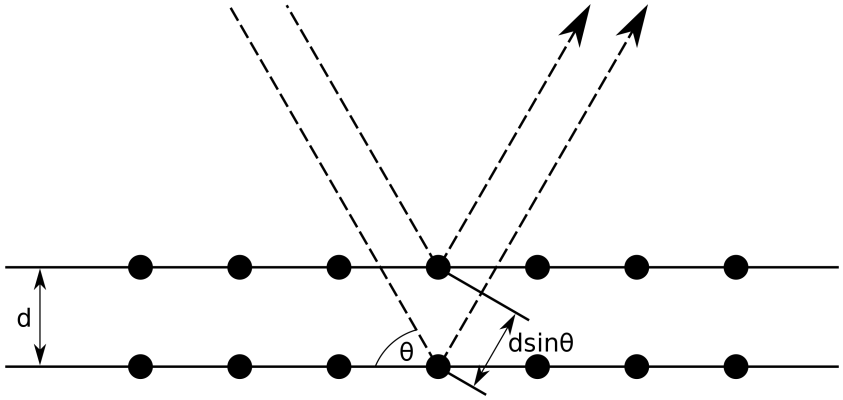

Figure 5: Bragg's law for atoms of a crystal structure from [15]

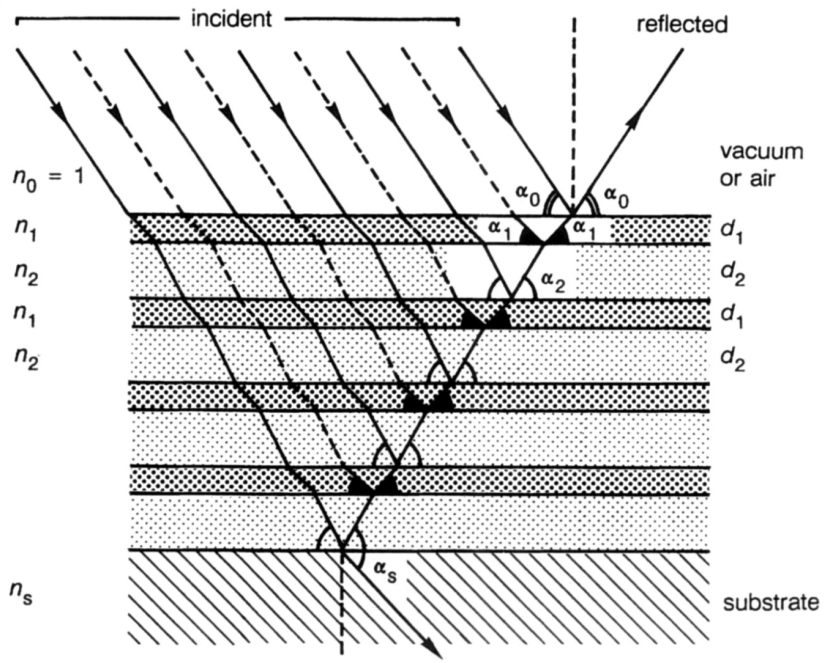

Figure 6: Working principle of a multilayer monochromator from [13]

2.2 Interaction of X-rays with Matter

The energy E of an X-ray photon is described by:

$$E = h\nu = \frac{hc}{\lambda} \tag{4}$$

with h being the Plack constant, c being the speed of light, ν being the frequency and λ being the wavelength of the X-ray. X-rays, being part of the electromagnetic spectrum can

interact with matter in the following ways:

2.2.1 Photoelectric Absorption

If the energy of the impinging X-ray is larger than the binding energy of a bound electron of the atom, the electron can be ejected. If the ejected electron is in a lower energy state than other bound electrons, the void left by the ejected electron can be filled by electrons of a higher energy state. The energy difference between the different bound states of this process, can be compensated by emitting electromagnetic radiation, i.e. a fluorescence photon. Alternatively the energy difference can be compensated emitting another electron from the atom. This emitted electron is called an Auger electron. The information about the likelihood distribution of this two competing processes is given in the fluorescence yield:

$$\omega = \frac{Z^4}{A + Z^4} \tag{5}$$

with Z being the atomic number, A being a factor for the different possible transition series (e.g. K, L, M, see section 2.1.2) and the fluorescence yield ω giving the relative probability of emitting a fluorescence photon. For X-ray fluorescence analysis (XRF) a high fluorescence yield is beneficiary. The increase of the fluorescence yield for high atomic numbers is shown in figure 7.

2.2.2 Elastic Scattering

Photons can interact with bound electrons without transferring energy. This process is called elastic or Rayleigh scattering. Still the intensity of the scattered radiation changes, because of the change of direction of the radiation. The intensity of the scattered radiation of primary intensity I_0 is given by

$$I_{coh} = I_0 r_e^2 \left[\frac{1 + cos^2\theta}{2} \cdot f^2\left(\frac{sin\theta}{\lambda}, Z\right) \right] \tag{6}$$

with θ being the scattering angle, $f^2\left(\frac{sin\theta}{\lambda}, Z\right)$ being the atomic form factor for incident radiation of wavelength λ and a single atom of the atomic number Z. [16]

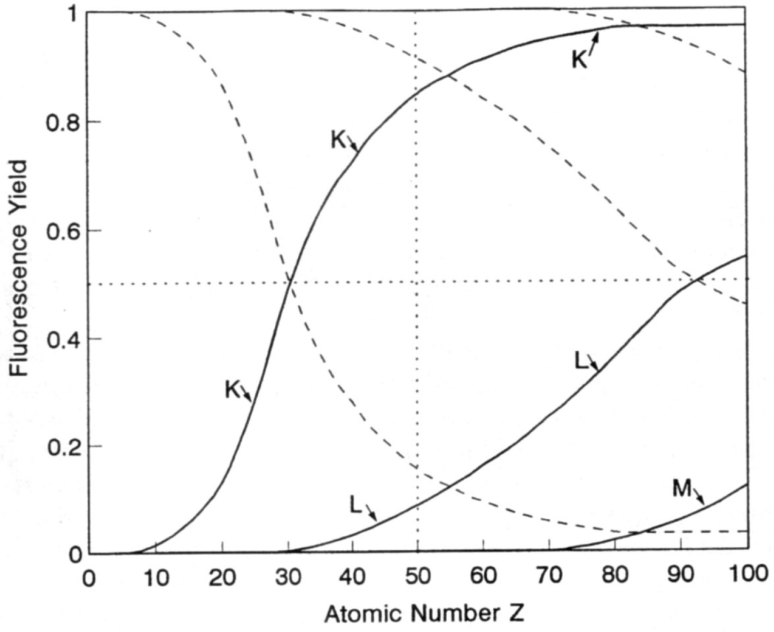

Figure 7: Fluorescence yield for K-,L- and M-Lines for different atomic numbers from [13]

2.2.3 Inelastic Scattering

Photons can also interact with electrons transferring energy. This process is called inelastic or Compton scattering. The wavelength shift of this process can be calculated by considering energy and momentum conservation for this process. This leads to:

$$\frac{E_a}{E_b} = \left[1 + (1 - cos\psi)\frac{E_b}{E_e}\right]^{-1} \tag{7}$$

with E_a being the energy of the photon after the scattering, E_b the energy of the photon before the scattering, ψ the scattering angle and E_e the rest energy of the electron ($\approx$ 0,511 MeV). Therefore the wavelength shift is given by:

$$\lambda_a - \lambda_b = \lambda_C(1 - cos\psi) \tag{8}$$

with λ_C being the Compton wavelength of the electron. Compton scattering is always incoherent.

2.2.4 Pair Production

Electromagnetic radiation with an energy higher than 1,02 MeV can interact with the atomic nucleus creating an electron positron pair. Since this process is only possible for high energy X-rays and heavy nuclei, this process can be neglected for most X-ray fluorescence applications, because the energy of the exciting radiation is in the keV range. These processes,

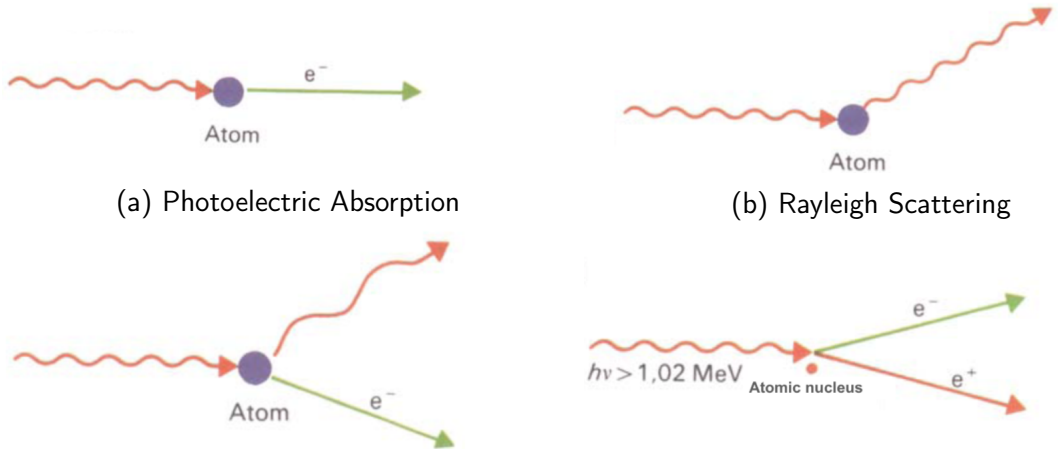

(a) Photoelectric Absorption (b) Rayleigh Scattering

(c) Compton Scattering (d) Pair production

Figure 8: Possible ways of interaction between X-rays and Matter from [17]

also depicted in figure 8, lead to the attenuation of radiation in matter. This attenuation is described by the Beer-Lambert law:

$$I(d) = I_0 \cdot e^{-\mu \cdot d} = I_0 \cdot e^{-(\frac{\mu}{\rho}) \cdot \rho \cdot d} = I_0 \cdot e^{-\frac{\mu}{\rho} \cdot \frac{m}{F}} \tag{9}$$

with I_0 being the intensity of the primary radiation, $I(d)$ being the intensity of the radiation after passing through the distance d of a material with a density ρ and $\frac{\mu}{\rho}$ being the mass attenuation coefficient. The linear coefficient μ is the sum of the different attenuation coefficients τ for photoelectric absorption, $\sigma_{elastic}$ for elastic scattering and $\sigma_{inelastic}$ for inelastic scattering:

$$\mu = \tau + \sigma_{elastic} + \sigma_{inelastic} \tag{10}$$

Photoelectric absorption and inelastic scattering can lead to the ionization of an atom, possibly leading to characteristic radiation (see section 2.1.2). This phenomenon is called X-ray fluorescence and, is exploited in X-ray fluorescence analysis (XRF) to investigate the properties of a material without destroying it.

2.3 X-ray fluorescence analysis (XRF)

The XRF method uses the phenomenon of characteristic radiation to investigate the elemental composition of a material. An X-ray source (e.g. X-ray tube, see section 2.1) emits X-rays at the sample material. The impinging X-rays ionize atoms via photoelectric absorption or inelastic scattering (see section 2.2), by ejecting inner-shell electrons from the atoms. Electrons in higher energy states can fill the void, left by the ejected electron emitting characteristic radiation (see section 2.1). This destruction free method, can be realized with setups of multiple different geometries using various ways of detection.

2.3.1 Energy dispersive X-ray fluorescence analysis (EDXRF)

Energy dispersive X-ray fluorescence analysis (EDXRF) converts the fluorescence signal into an electric signal proportional to the energy of the fluorescence signal. The classical EXRF setup usually needs very little to no sample preparation, and can be realized without a special measurement environment (i.e. vacuum chamber). Still in some cases it can be useful to conduct the measurements in a vacuum chamber. Elements with low atomic number for example, have a low fluorescence yield (see figure 7) and therefore create a weak fluorescence signal, which can easily be absorbed / distorted by air. Classical EDXRF uses a source-detector-setup, where both source and detector are at a 45° angle with the sample surface, as can be seen in figure 9.

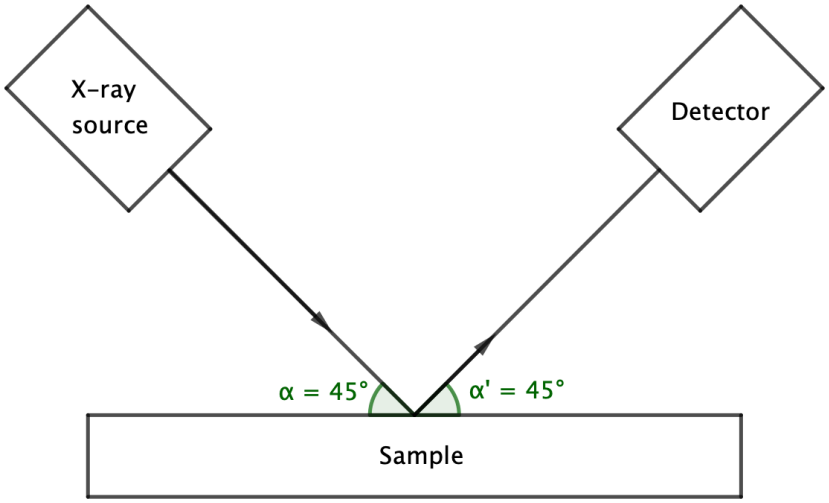

Figure 9: Classical EDXRF setup

Commonly semiconductor detectors in general, and silicon drift detectors in particular are used as detectors (This is also the case for both measurement setups used for this diploma thesis, see sections 4.1.1 & 4.1.2).

Silicon Drift Detector (SDD) The working principle of semiconductor detectors exploits ionization of semiconductor atoms by radiation (i.e. X-rays). As depicted in figure 10, in a silicon drift detector (SDD) impinging X-rays ionize atoms in a the detector material (high purity silicon), thereby creating electron clouds with a charge proportional to the energy of the radiation. An electric field, created by concentric drift electrodes, then accelerates the electron cloud towards an anode at the center of the electrodes, thus creating a signal peak proportional to the energy of the detected radiation [18].

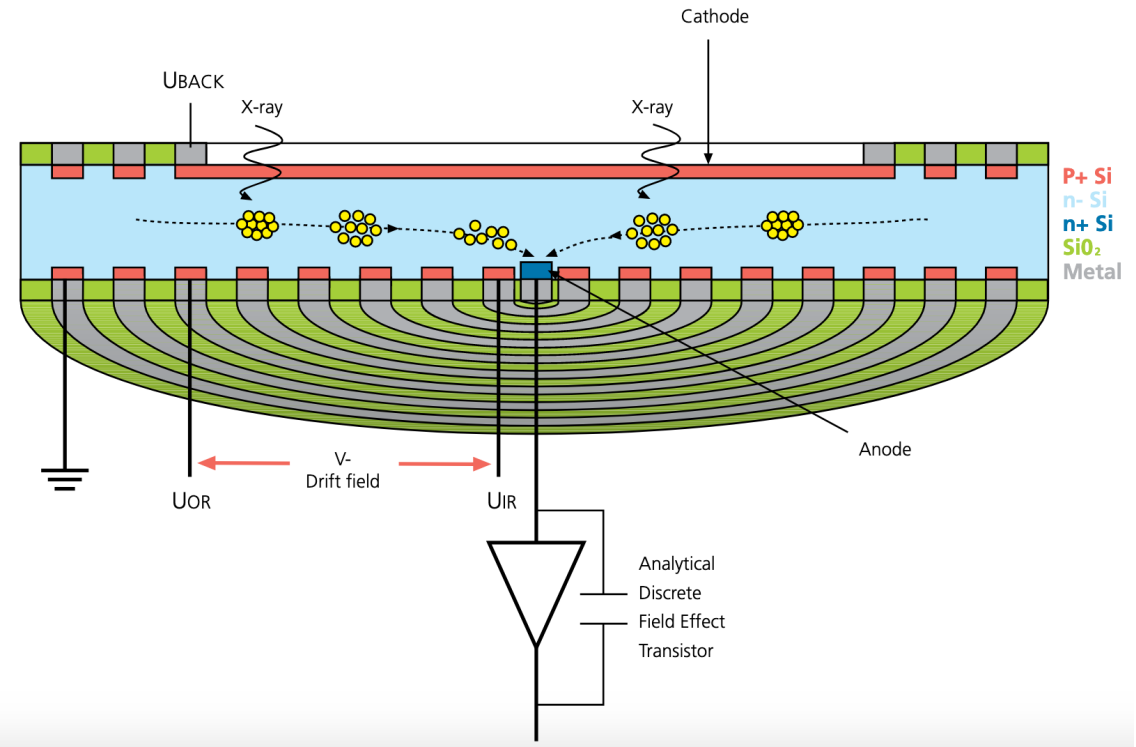

Figure 10: Working principle of a silicon drift detector (SDD) from [18]

Dividing the range of signals into channels and counting the number of signals in a specific channel leads to a spectrum, which can be converted to an energy spectrum with the correct calibration. For a more detailed explanation of semiconductor detectors and EDXRF see [11, 18].

2.3.2 Total-reflexion X-ray fluorescence analysis (TXRF)

Total reflexion X-ray fluorescence analysis (TXRF) is a geometric setup for XRF, where the low divergent primary radiation is directed at the sample material, with a smooth flat surface, at a very small angle close to the critical angle (see figure 11). Because of the small

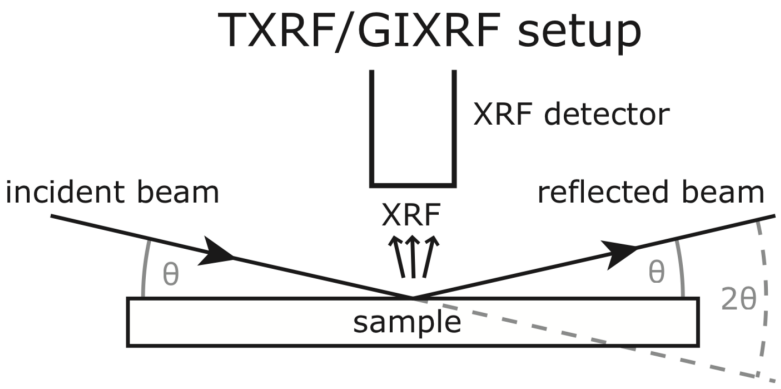

Figure 11: Geometric setup of Total reflexion X-ray analysis (TXRF) and Grazing incidence X-ray analysis (GIXRF) from [7]

penetration depth of the primary radiation and the double excitation of the atoms, by the primary beam and the reflected beam (see section 2.3.2), the fluorescence signal, which in this setup is detected right above the focal spot of the X-ray source, as can bee seen in figure 11 is highly increased. At the same time the background is reduced, because of the reduced penetration of the radiation into the sample carrier. Thus TXRF is a highly sensitive method.

Critical angle of X-rays For X-rays, any medium is optically less dense than vacuum and any solid is optically less dense than air, which is in contrast to visible light [13]. The effect of total reflexion occurs only on smooth flat surfaces. The total reflexion of X-rays at a solid is a result of the refractive index n of a material for X-rays with the wavelength λ being a complex parameter:

$$n = 1 - \delta - i\beta \tag{11}$$

with:

$$\delta = \frac{\lambda^2}{2\pi} r_e \rho_e = \frac{\rho N_A r_e \lambda^2}{2\pi A} f_1^0(\omega) \qquad \text{and} \qquad \beta = \frac{\lambda}{4\pi}\left(\frac{\mu}{\rho}\right)\rho = \frac{\rho N_A r_e \lambda^2}{2\pi A} f_2^0(\omega) \tag{12}$$

with r_e being the classical electron radius, ρ_e being the elctron density and ρ being the density of the material, N_A being the Avogadro constant, A being the atomic weight, $\left(\frac{\mu}{\rho}\right)$ being the mass attenuation coefficient (see section 2.2) and $f_1^0(\omega)$ being the real part and $f_2^0(\omega)$ being the complex part of the atomic scattering factor in forward direction. The critical angle can be estimated by (for calculation see [13]):

$$\alpha_{crit} \approx \sqrt{2\delta} \tag{13}$$

X-ray standing wave field (XSW) The total reflexion of the primary radiation, in one of the sample layers or the substrate, leads to interference between the incoming and reflected waves. Because of this a standing wave field of X-rays forms above the interface of total reflexion (see figure 12).

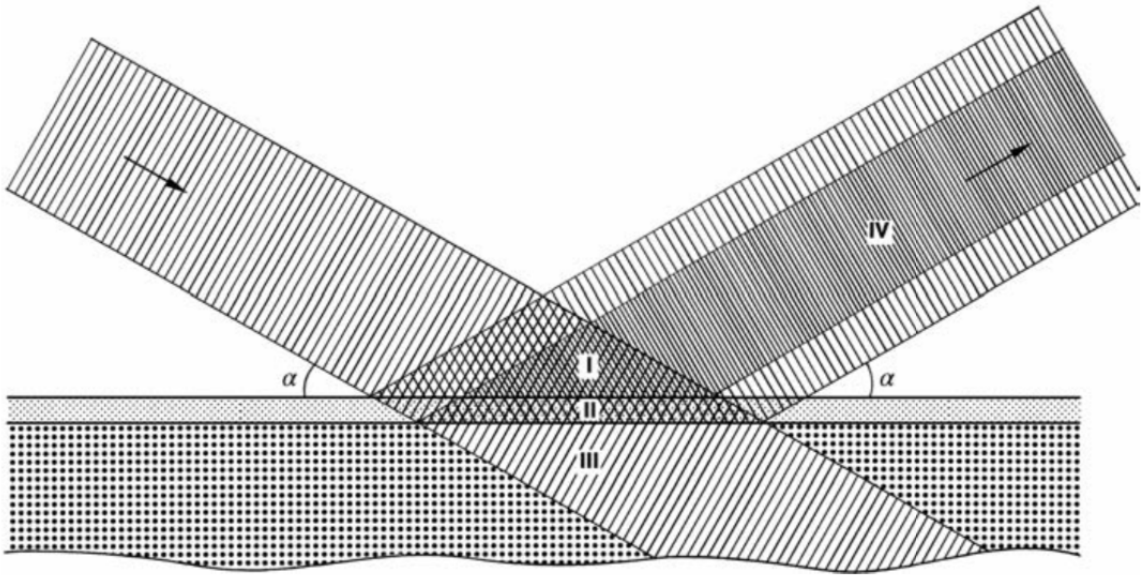

Figure 12: X-ray standing wave for a single thin layer deposited on a thick substrate. Standing waves appear in the triangular region I and in the trapezoidal region II. Regions IV shows a simple propagating wave with an angle-dependent amplitude. Taken from [13]

The angle dependence of the amplitude of this standing wave field and the intensity of the radiation in the substrate is depicted in figure 13.

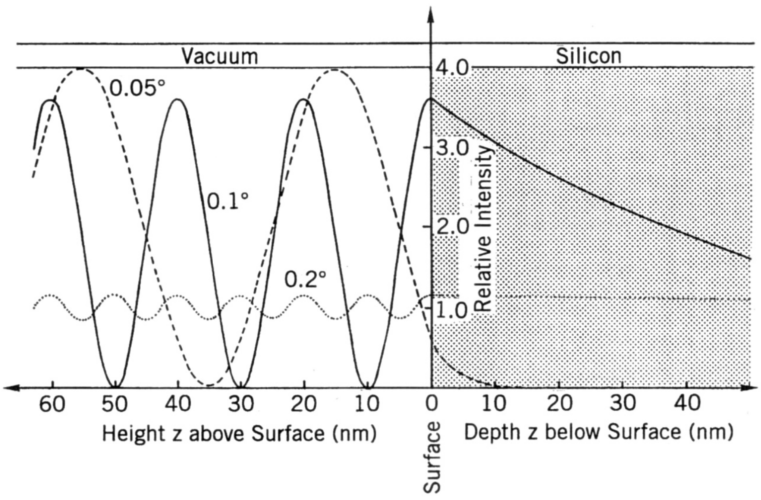

Figure 13: Angle dependent X-ray intensities above and in a thick substrate from [13]

2.3.3 Grazing incidence X-ray fluorescence analysis (GIXRF)

Grazing incidence X-ray fluorescence analysis (GIXRF) utilizes the angle dependence of the X-ray standing wave field (XSW, see section 2.3.2), to investigate not only the composition of a probe as in XRF in general, but also the depth profile of the sample, by varying the angle of incidence around the critical angle. This setup (see figure 11) produces different angle dependent fluorescence intensities for different layer thicknesses, shown in figure 14.

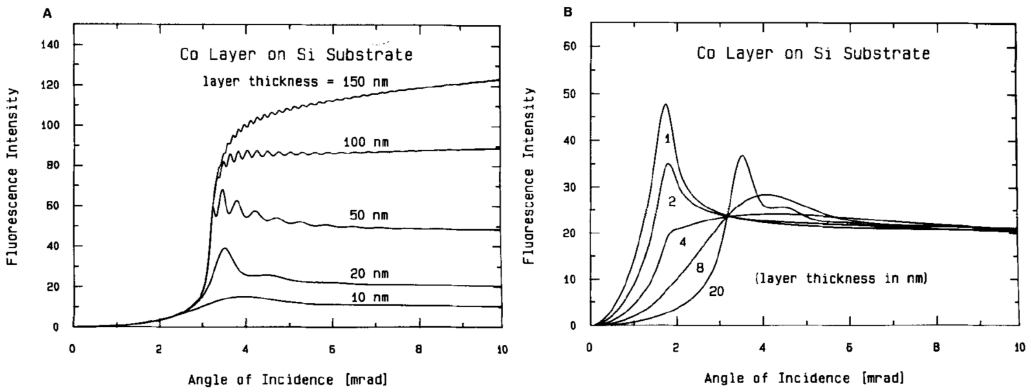

(a) Calculated Intensities for different layer thicknesses for a Co layer

(b) As in (a), but normalized to intensities for large angles of incidence

Figure 14: Calculated fluorescence intensity as function of the angle of incidence for different layer thicknesses of a Co layer from [19]

Still the evaluation of GIXRF signals produces ambiguous results (see [7]), as shown in

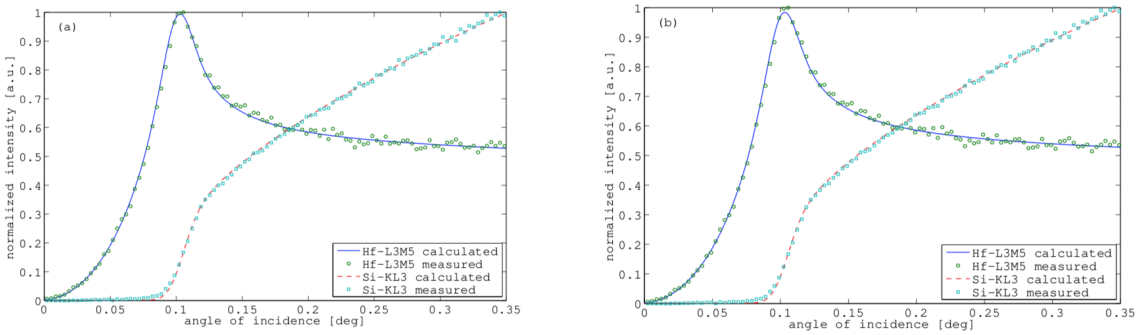

(a) Using a material with density 6.1 g/cm^3 and thickness 2.25 nm

(b) Using a material with density 6.7 g/cm^3 and thickness 2.05 nm

Figure 15: Fluorescence signal for Hf and Si from a $HfSiO_x$ layer, calculated using only a GIXRF signal. Good fit results are obtained for (a) as well as (b), thus showing the ambiguity of the GIXRF data. Taken from [7]

figure 15, making it necassary to combine GIXRF with other measurement techniques to find an unambiguous sample model, as solution to the measurement problem.

2.4 X-ray reflectometry (XRR)

X-ray reflectometry is a non-destructive method to investigate thickness and roughness of thin layers. Varying the angle of incidence around the critical angle (see section 2.3.2), the reflected intensity reaches periodic minima and maxima, shown in figure 16. These, so called Kiessig fringes are a result of interference phenomena, of radiation reflected on different interfaces and can be used to determine the thickness of the investigated thin layers. The distances between the maxima or minima can be calculated for a single thin layer by (see [13]):

$$\Delta\alpha = \frac{\lambda}{2d} \tag{14}$$

with $\Delta\alpha$ being the distance between neighbouring maxima / minima, λ being the wavelength of the radiation and d being the thickness of the investigated layer. As shown in figure 16 this, together with Bragg's law (see equation 3) can be used to calculate the layer thicknesses of multilayer structures.

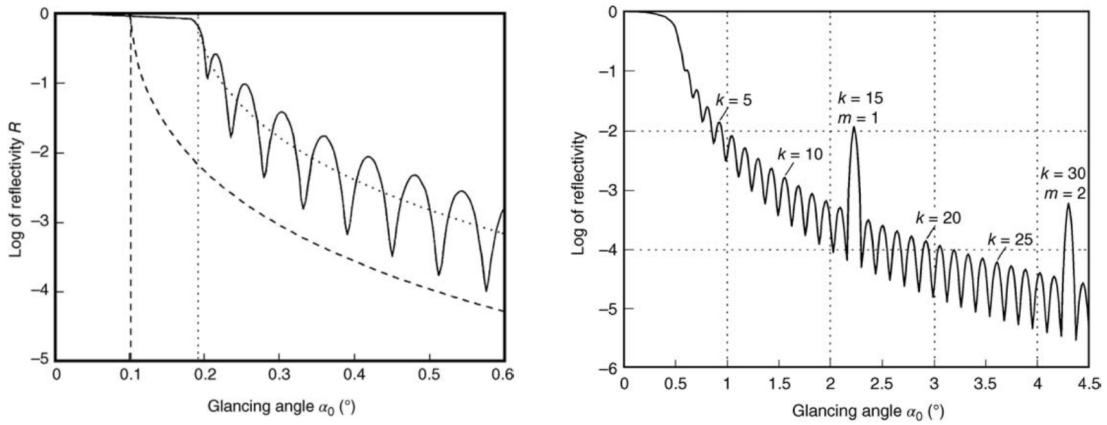

(a) Reflectivity of a thin 30 nm cobalt layer on a thick silicon substrate.

(b) Reflectivity of a multilayer,consisting of 15 bilayers of platinum and cobalt, each of them 1.9 and 0.2nm thick. The lower Kiessig maxima k can easily be distinguished from the higher Bragg maxima with m = 1 and m = 2.

Figure 16: Angle dependent reflectivity from [13]

2.5 Glancing incidence X-ray analysis (GIXA)

In 1993 de Boer and van de Hoogenhof proposed a set of combined measurement methods, for setups with a small angle of incidence of the primary radiation, naming the combined measurement Glancing Incidence X-ray analysis (GIXA). Following the combined GIXRF & XRR approach proposed by them, Ingerle [7], built a tabletop spectrometer, allowing both measurements to be done at the same time in a single device (see figure 17).

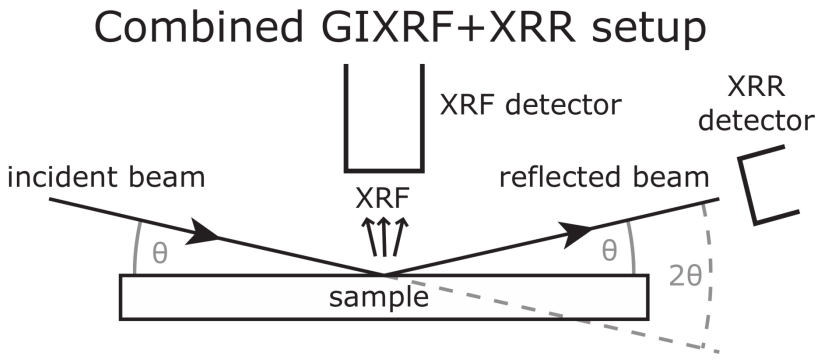

Figure 17: Combined GIXRF & XRR setup from [7]

To evaluate the data, taken this way he started the jGiXa software project, following de

Boers appoach for the calculation and fitting the calculated intensity distribution to the measurements. For a detailed explanation of the calculation see [1, 7]. The calculation parametrizes the sample model, of a multilayer sample, to j layers of a specific material composition, thickness d and roughness σ (see figure 18).

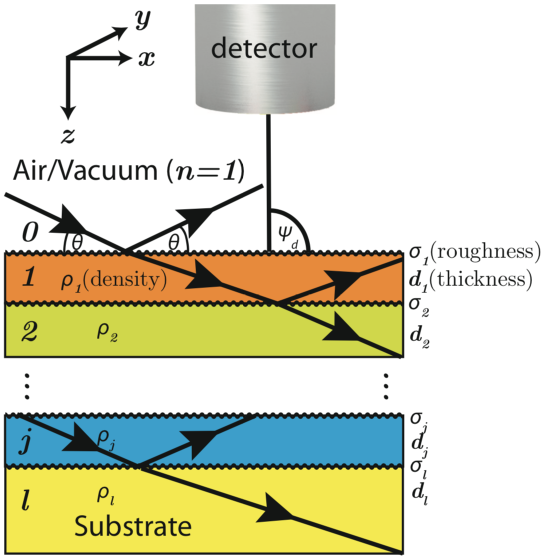

Figure 18: GIXRF setup for a multilayer sample with j layers, with thickness d and roughness σ from [7]

2.5.1 Roughness

The roughness in this model is given as a parameter σ, being the root mean square of vertical deviations from a perfect plane. The model uses σ to calculate an adjustment factor for the amplitudes of the reflected and transmitted electromagnetic waves of each interface [7, 1]. This model is depicted in figure 19.

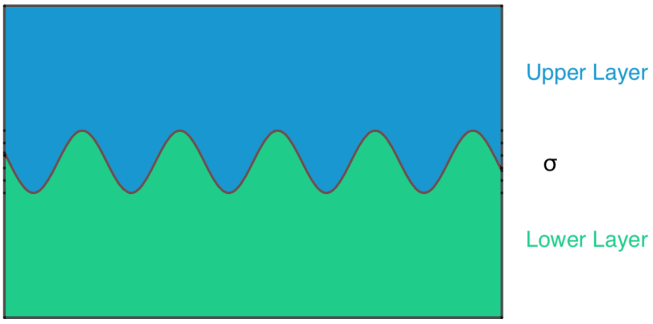

Figure 19: Roughness represented by a single parameter σ

A second approach based on [21, 20], representing the roughness as independent thin layers between two layers with a continuous transition of the refractive index was implemented for the work of this diploma thesis (see sections 3.6 & 4.2.1 & 4.2.2). This transition of refractive index can be modeled by creating layers with a continuous transition of material composition and density. For example: the roughness of an interface of two layers, e.g. Ti with a density of 4.5 g/cm^3 and Si with a density of 2.3 g/cm^3 can be represented by adding a number of intermediate layers, e.g. 4 to the sample model:

- $Ti_{0.8}Si_{0.2}$ with a density of 4,06 g/cm^3
- $Ti_{0.6}Si_{0.4}$ with a density of 3.62 g/cm^3
- $Ti_{0.4}Si_{0.6}$ with a density of 3.18 g/cm^3
- $Ti_{0.2}Si_{0.8}$ with a density of 2,74 g/cm^3

Since the density is not clearly given from the material composition, but is also dependent of the atomic packing factor, the transition of material composition and density should be decoupled and calculated independently (see section 3.6).This model is depicted in figure 20.

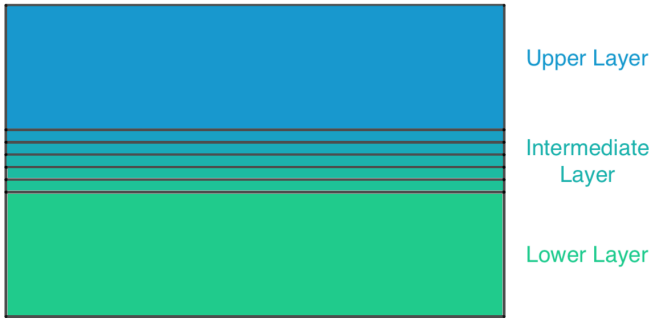

Figure 20: Roughness represented by a number of intermediate layers, continuously transitioning from one material composition / density to the other.

3 Development of jGiXa

jGiXa is an academic Java software project. The acronym stands for ***java Glancing incidence X-ray analysis software***.

3.1 jGiXa 1.0

jGiXa was initially developed by Ingerle [7, 2], to match the requirements of combined GIXRF and XRR analysis as proposed by de Boer [1]. The software originally consisted of two parts. The calculation of the spectra was written in Java, to benefit from Javas easy to use parallelization options. The graphical user interface and the global optimization algorithms were written in MatLab, to use the powerful global optimization libraries implemented in MatLab. The basic working principle of the software is shown in figure 21.

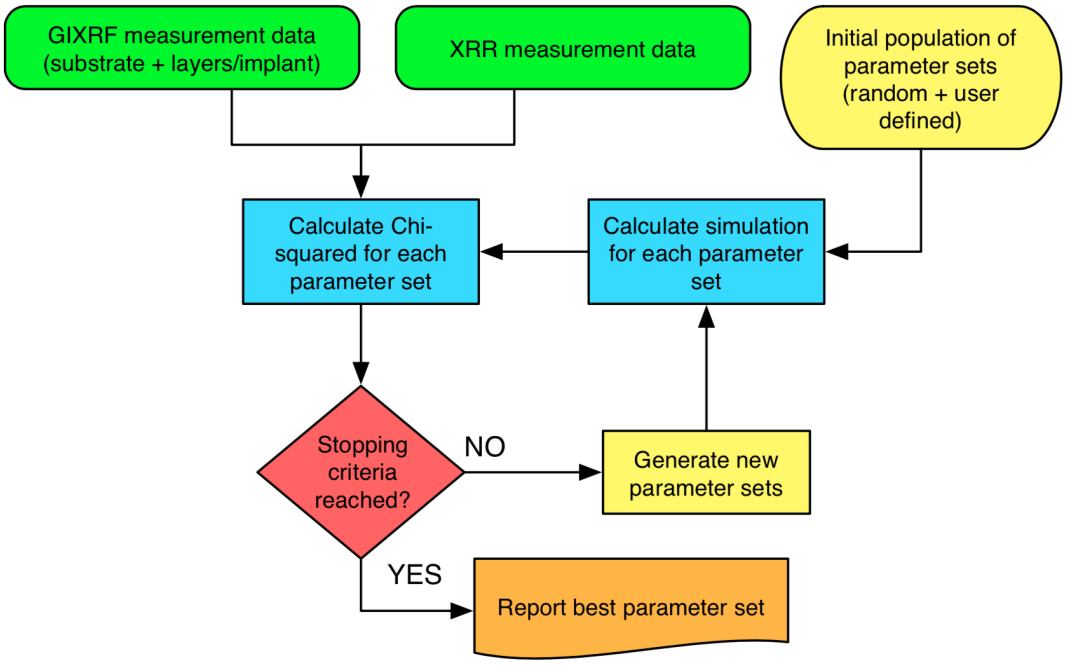

Figure 21: Flow chart illustrating the working principle of jGiXa from [7]

Over time it became clear that this separation, will make it hard to maintain a useable version of the software, as Java and MatLab develop over time as does jGiXa.

3.2 jGiXa 2.0

In the first part of this diploma thesis a Java based graphical user interface and a working global optimization algorithm were implemented into the Java part of the jGiXa software package, allowing jGiXa to work as a standalone Java software. This is advantageous in respect to :

- Portability / Budget: Both Java and MatLab are available for all platforms. Still keeping both up to date and the complete code working for the latest versions is more demanding than for a single Java application. Also while all necessary Java packages and a JRE are free to use, MatLab is a commercial software product, with an annual license cost of 800 €.

- User friendliness / Performance: An improvement of speed by a factor 6 was achieved (see section 4.3). This performance boost from multiple hours per optimization, to less than an hour per optimization, leads to a better workflow, allowing the user to adjust the sample model and rerun the optimization multiple times on the same day. Also the introduction of tooltips allow sporadic users a more intuitive use of the application.

- Maintainability / Scalability: The new structure of the project allows people familiarizing themselves with the code not to know both programming languages, and to get a much quicker clear overview of the complete structure of the code, thus allowing the maintenance and further development of the software to be done by project students.

Without going into too much detail it should be mentioned here that the graphical user interface (GUI) was constructed using the MVC design pattern [10], separating data model, presentation and control. The data model mirrors the internal data model used for the calculation while leaving room for object manipulation. More detailed information about the concrete structure of the code is given in the Javadoc of the project. The GUI is separated into three frames for experimental setup, sample model and optimization. The Main window of the application is shown in figure 22. The different frames and subframes are explained below. The input of the complete project, the setup, the sample and the optimization can be saved / loaded separately to / from files in XML file format. For a better user experience the files have custom filename extensions (*.jpr* (jGiXa Project), *.jse* (jGiXa-Setup), *.jsa* (jGiXa Sample), *.jop* (jGiXa-Optimization)), only showing files of the correct type, while loading.

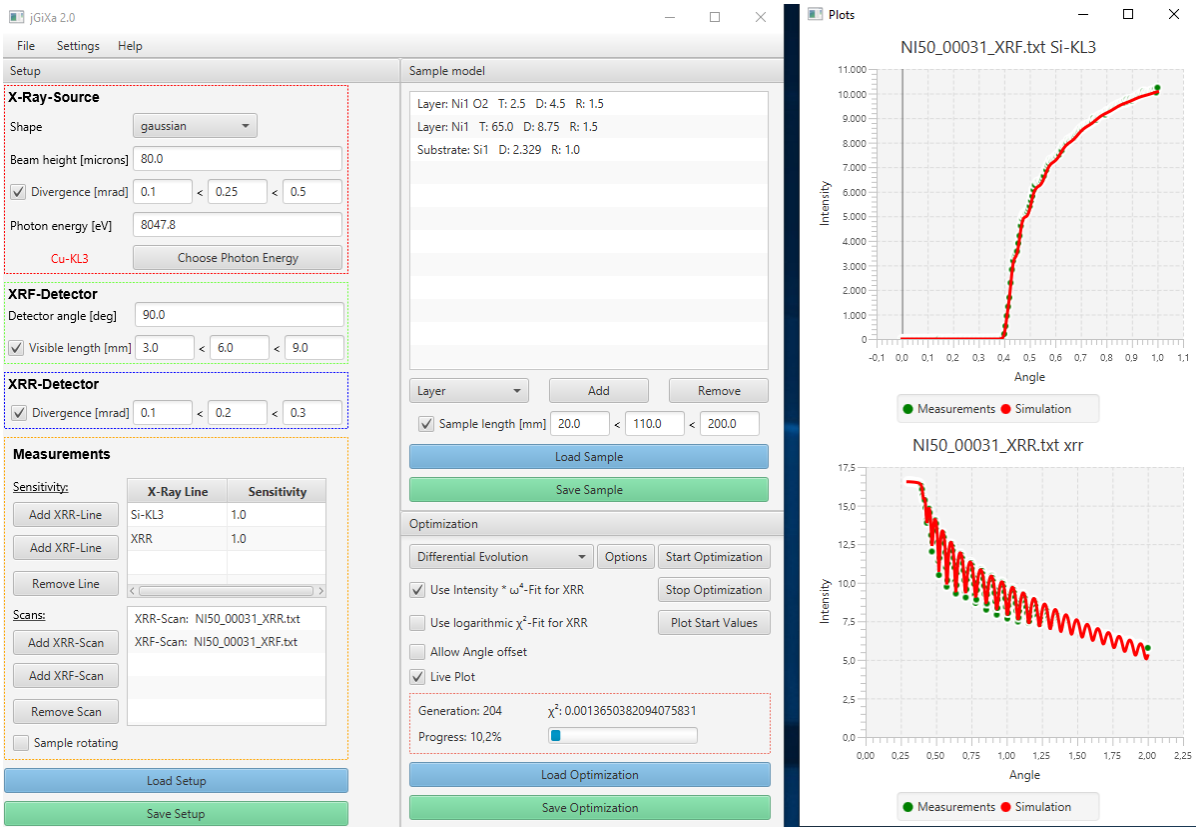

Figure 22: Main Frame of the jGiXa application, while running with Live Plot activated.

3.3 Setup

To parameterize the setup jGiXa offers the following options (see figure 23):

- **Shape, Beam height & Visible length** are parameters, to consider the fact that the primary beam is not infinitely small, and therefore the illuminated area is highly dependent of the angle of incidence. jGiXa calculates the illuminated area (beam footprint), using the **Beam height** parameter and the angle of incidence. The primary intensity distribution of the beam, from the center is given by the **Shape** parameter. As can be seen in figure 24, the beam footprint becomes large for small angles, thus exceeding the detector area, while for large angles the incoming radiation produces a small footprint with a sharp intensity peak. To consider this unbalance the **Visible length** parameter normalizes the calculated intensities to a beam footprint of an area visible to the detector with a uniform intensity distribution. At this point it should also be mentioned that jGiXa's user interface offers to check and uncheck certain parameters. While checked parameters, become variables of the optimization and vary

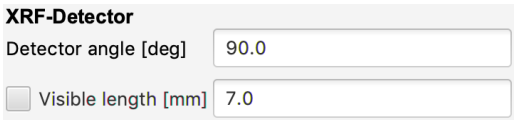

(a) XRF-Detector

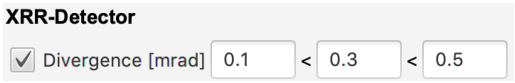

(b) XRR-Detector

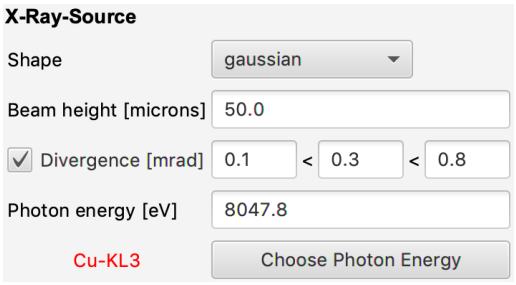

(c) X-Ray-Source

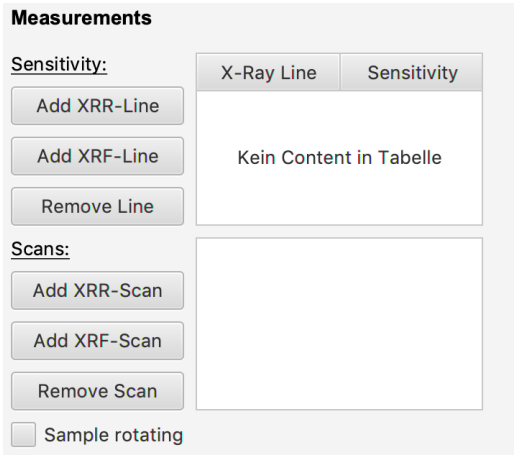

(d) Measurements

Figure 23: Screenshots of the subframes of the setup frame of the GUI.

between the left (minimum) and right (maximum) values, starting with the middle value, unchecked parameters use the value in the according textfield for the calculation.

- **Photon energy** is the monochromatic energy of the primary radiation, and can either be entered manually or chosen from a database with the characteristic lines for different elements.

- **Divergence for X-ray Source & XRR Detector** are parameters dealing with the angle distribution of the primary and secondary radiation (see figure 25). As shown in figure 25 the primary radiation hits the target at different angles and again is detected at different angles. These effects are taken into consideration, by convoluting the calculated curve with a gaussian distribution. Different divergences have to be used for XRF and XRR intensities, due to the reflected beam usually being shaped by additional optic in front of the detector, thus having a smaller divergence [7]. The divergence entered in the X-ray source subframe is used to convolute the fluorescence signal and the divergence entered in the XRR-Detector subframe is used to convolute the reflectivity signal. The effect of this convolution is shown in figure 26.

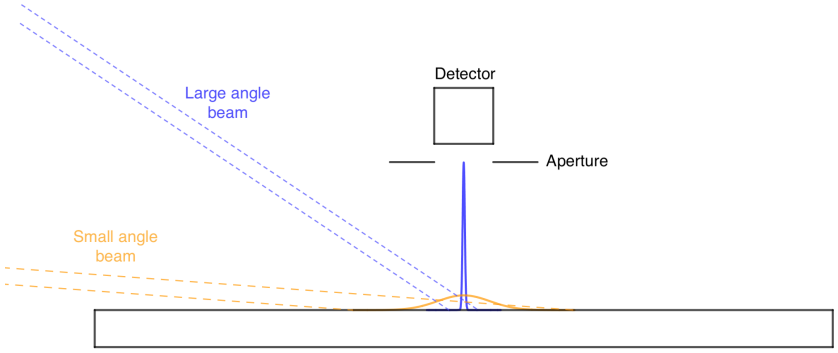

Figure 24: Depiction of the Visible Length Parameter. For large angles of incidence (blue) the beam footprint is small with a sharp peak, while for small angles (orange) the beam footprint becomes large, with a more uniformily distributed intensity.

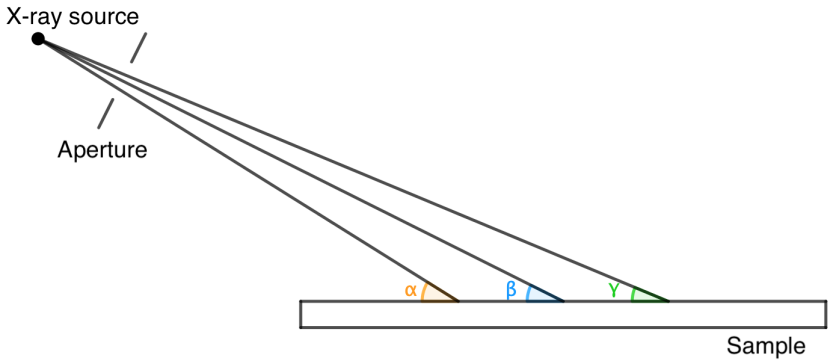

(a) Angular divergence of the primary radiation

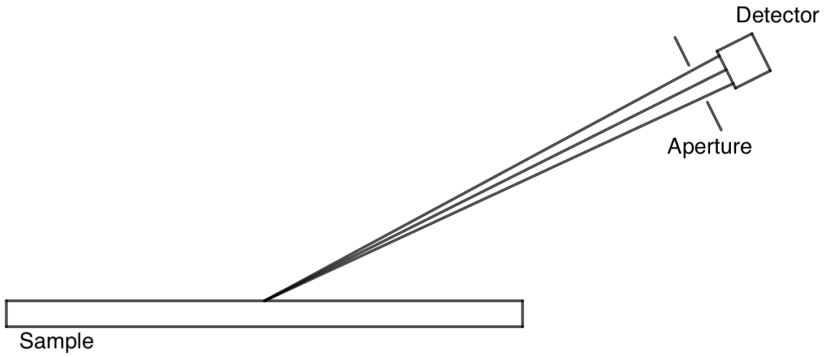

(b) Angular divergence of the secondary radiation

Figure 25: Depiction of the Divergence Parameter

- **Sensitivity** is a factor to consider the sensitivities of the different X-ray lines. The lines can be chosen from a database.

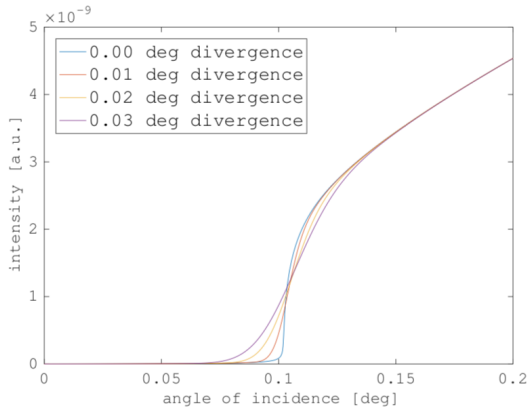

(a) GIXRF of a bulk material

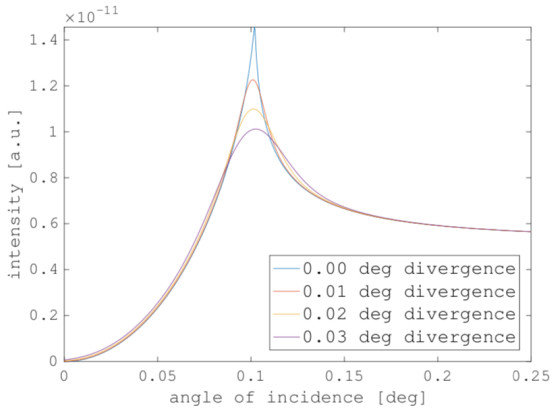

(b) GIXRF of a thin layer

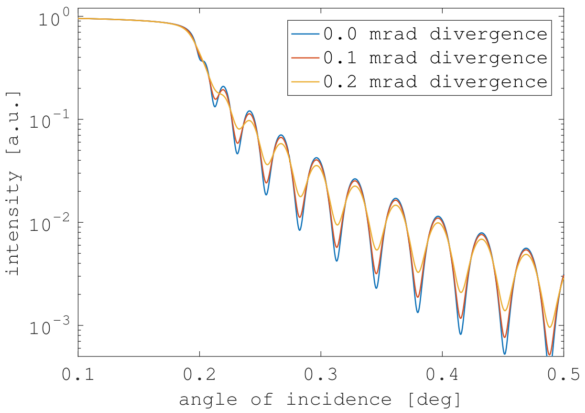

(c) XRR

Figure 26: Influence of angular divergence on the calculation from [7]

- **Scans** allows to import the measurement data from *.txt* files, with the angle dependent intensities of the different lines.

- **Sample rotating** allows to choose between a setup with a sample that is rotating in relation to X-ray-Source and detector (e.g. synchrotron setup) and a setup with a moving X-ray source and a fixed angle between sample and detector(e.g. lab setup).

3.4 Sample

The sample model can be built by adding, removing, moving or editing the following components:

- **Layer** is a single layer with a parameter set including: **thickness**, **density**, **roughness**

and a parameter for each **element** in the material composition. Each parameter can be checked as an variation parameter.

- **Stack** is a periodic succession of layers or stacks, with a list for the stack model similar to the list for the sample model and an additional parameter for the number of **repeats**.
- **Intermediate Layer** is a succession of layers continuously transitioning between its upper and lower layer. Separate transition functions for density and material composition can be used, possible options being a **linear** transition function and a **fermi**-distribution-like transition function (see section 3.6).

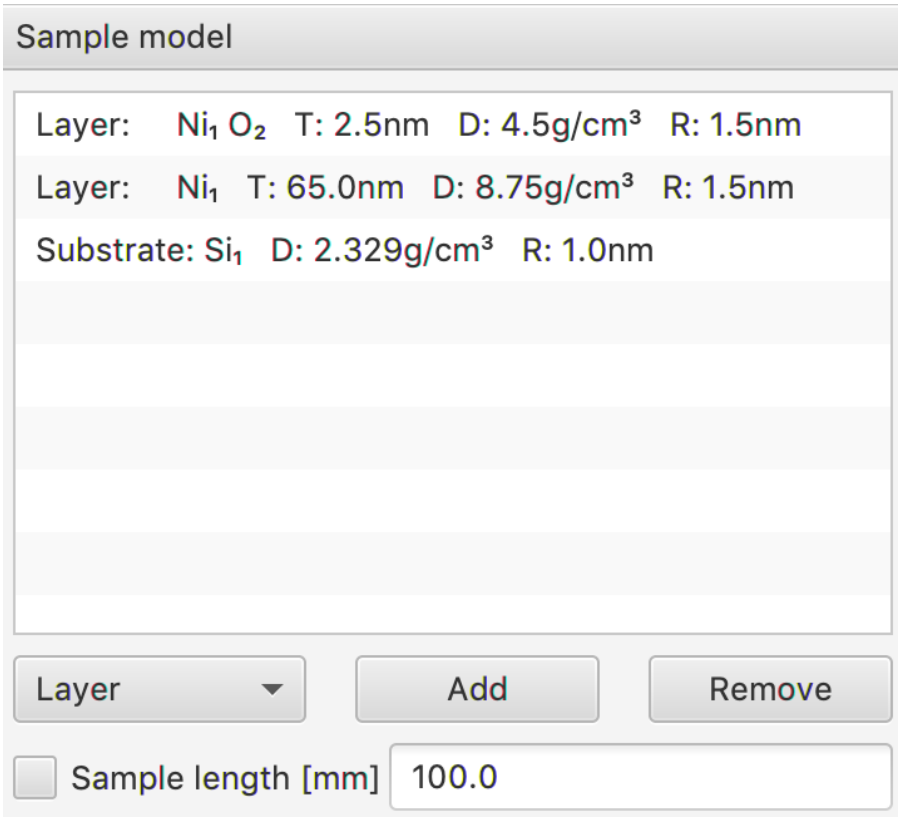

Figure 27: Screenshot of the sample frame of the GUI.

The sample is further parameterized by:

- **Sample length** corrects the reflectivity for small angles where the beam footprint (see **Shape, Beam height & Visible length**) exceeds the length of the sample. The effect of this correction can be seen in figure 28.

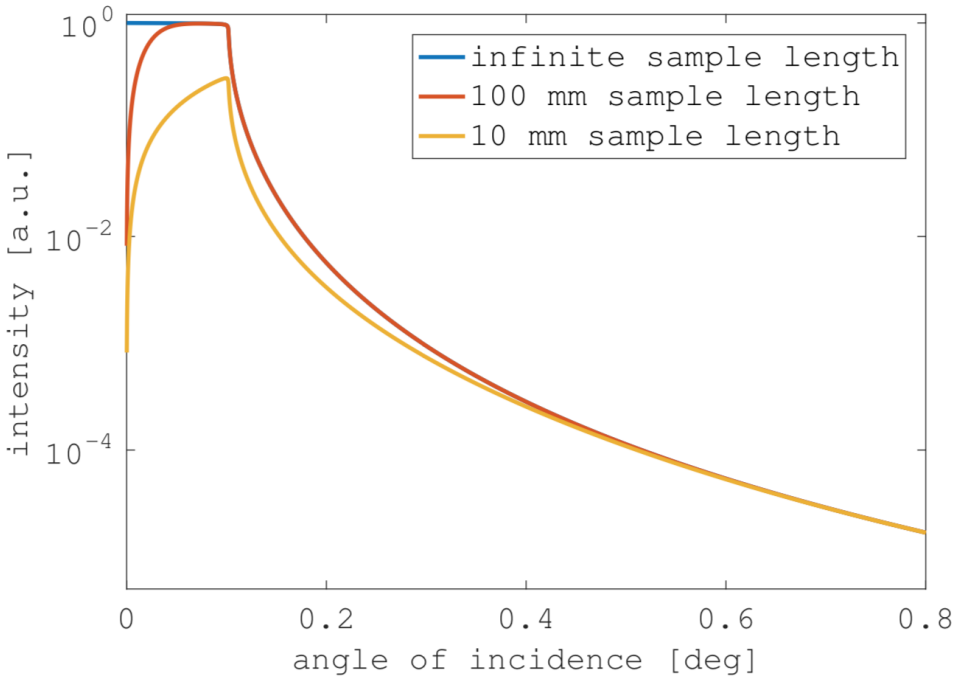

Figure 28: Influence of the sample length from [7]

3.5 Optimization

The general optimization menu (see figure 29) offers several options independent of the chosen optimization algorithm (specific parameters for the already implemented differential evolution algorithm are discussed in chapter 4.4):

- **Use $Intensity \cdot \omega^4$ for XRR & Use logarithmic χ^2-Fit for XRR** are options to balance the fit. As can be seen in figure 21, the optimization algorithm generates solutions and compares their quality by calculating a weighted χ^2 value, only allowing improved solutions with a better χ^2 than its predecessor and discarding the others. The cumulated χ^2 for each curve is weighted (i.e. divided) by the maximum measured intensity value of the curve. The measured XRR intensities attain values spanning over several orders of magnitude (see logarithmic scale of figure 16), thus biasing the optimization towards solutions fitting the XRR-curve very well for small angles, where the XRR intensities are very large, but relatively neglecting solutions with good fits for large angle values, where the XRR intensities are several orders of magnitude smaller than for small angles. To deal with this problem, jGiXa allows to balance the fit by either multiplying simulated and measured intensities with the according ω^4 values, where ω is the angle of incidence, or calculating the weighted χ^2 not for the intensities

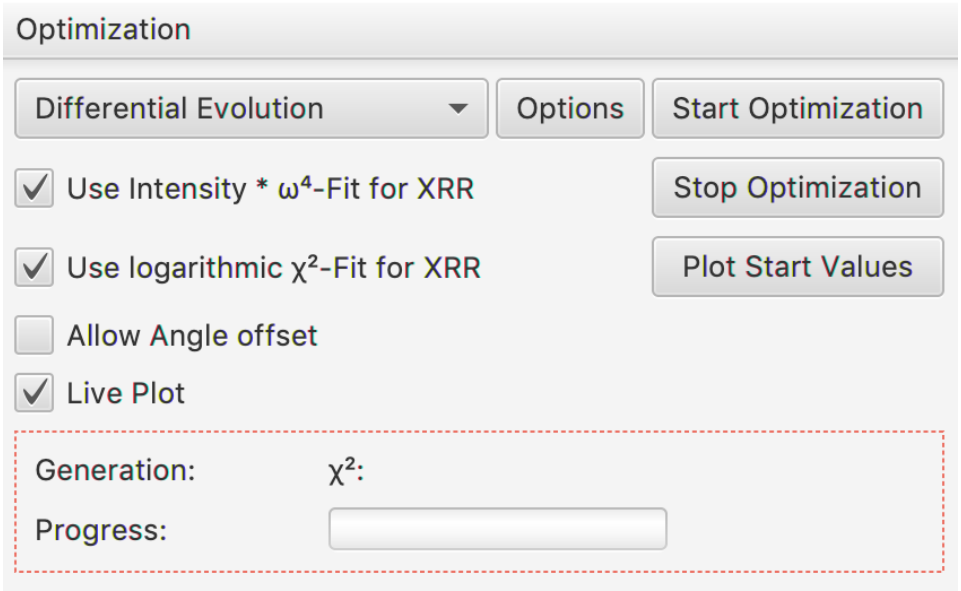

Figure 29: Screenshot of the optimization frame of the GUI

but their logarithms. While jGiXa allows to activate both options at the same time, it is recommended to choose only one of the options, since activating both seems not to provide correct solutions.

- **Allow angle offset** activates an optimization parameter that shifts the measured angles in positive or negative direction, to consider possible inaccuracies of the measured angle. Because even if activated this effect is expected to be very small, solutions with a large angle offset are penalized by the optimization by adding $e^{a^2} - 1$ to the weighted χ^2, with a being the angle offset.

- **Live Plot** activates a Plot window, that is updated every 10 iteration steps of the optimization algorithm, to graphically follow the progression of the optimization, while it is running. 10 iteration steps proved to be a good number to actively follow the optimization, without slowing it down.

3.6 Intermediate Layer

To expand jGiXa's ability to deal with roughness, a new roughness model (see section 2.5.1) was implemented, allowing a continuous transition of the refractive index of layers [21, 20]. This is achieved by creating layers with density and material composition transitioning from upper to lower layer. Since the density is not clearly given from the material composition, but

is also dependent of the atomic packing factor, the transition functions for both parameters can be decoupled and calculated independently. This new type of sample component called **Intermediate Layer** has the following parameter:

- **Thickness:** Like any regular Layer the thickness of an intermediate layer can either be variated or given as a fixed quantity.
- **Steps:** It is also possible to variate the number of steps, i.e. the number of created layers between upper and lower layer. Since the number of steps is merely a measure for the resolution of the transition function, and the variation of the number of steps slows the optimization down considerably, it is highly recommended to choose a fixed number of steps. Five steps seems to be a good choice to get a reasonably well resolution, without slowing the optimization down too much.
- **Transition functions for density & roughness:** The possible transition functions are either linear (see figure 30a) or a fermi distribution like function (see figure 30b) with the formula:

$$f(x) = \frac{1}{1 + e^{\frac{2 \cdot x - 1}{T}}} \tag{15}$$

with T being a parameter determining the form of the function, that can also be chosen as a variation parameter.

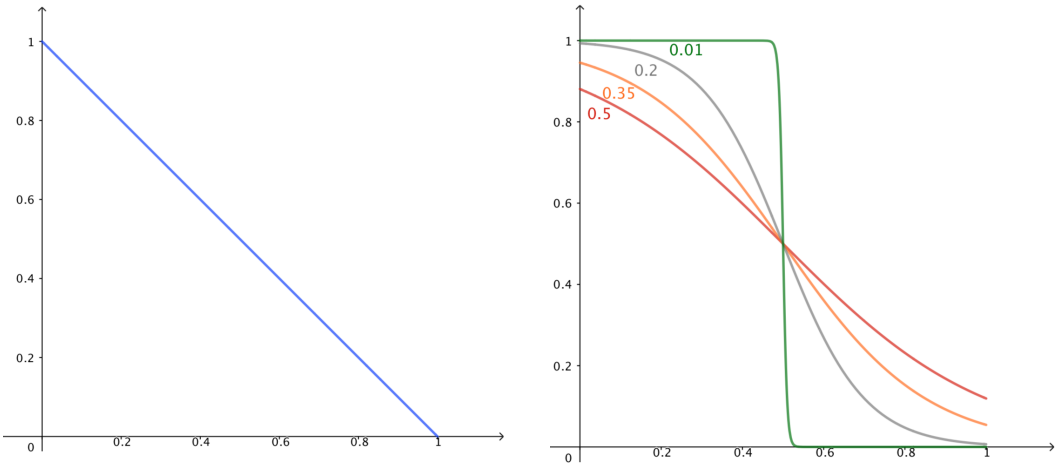

(a) Linear (b) Fermi for different T

Figure 30: Transition Functions

If an intermediate layer is the topmost layer of the sample model, jGiXa assumes an upper layer of vacuum. The new model was successfully tested for two Ti samples (see section 4.2).

4 Evaluation with jGiXa 2.0

4.1 Evaluation of a Ni sample with jGiXa 2.0

To test jGiXa 2.0, data of measurements of a Ni probe with a nominal thickness of 50 nm, measured with two different setups, was evaluated with the new software as well as the old software. To consider possible oxidation processes, the sample model was expanded by a thin Ni_1O_2 layer, with variable thickness, on top of the Ni layer. The exact sample model and optimization parameter are shown in tables 1 & 2.

Variated	Parameter	Minimum	Start	Maximum
✓	**Sample length** (mm)	20.0	110.0	200.0
Ni_1O_2				
✓	**Thickness** (nm)	0.0	2.5	5.0
✓	**Density** (g/cm^3)	1.0	4.5	8.0
✓	**Roughness** (nm)	0.0	1.5	3.0
Ni				
✓	**Thickness** (nm)	30.0	65.0	100.0
✓	**Density** (g/cm^3)	8.0	8.75	9.5
✓	**Roughness** (nm)	0.0	1.5	3.0
Si (Substrate)				
	Density (g/cm^3)		2.329	
✓	**Roughness** (nm)	0.0	1.0	2.0

Table 1: Sample model parameter for comparison evaluations

Parameter	Value
Optimization type	Differential evolution
Population size	100
Step size	0.85
Crossover probability	0.9
Strategy	rand1bin
Boundary constraints	bounceBack
Generations	2000

Table 2: Optimization parameter for comparison evaluations

4.1.1 Measurement from the X-Ray Center (XRC) of the TU Wien

The measurement 20160310_Ni50-00031a was taken at the X-Ray Center (XRC) of the TU Wien, using the following setup:

- **X-ray source:** Empyrean Cu LFF HR X-ray tube with maximum power rating 1.8 kW, focal spot 12 mm x 0.4 mm, exit window 300 µm beryllium, operated at 45 kV and 40 mA
- **Monochromator:** Hybrid monochromator consisting of a parabolical shaped graded multilayer and a channel-cut Ge(220) crystal
- **XRF detector:** Amptek XR-100SDD with Be entrance window, 25 mm^2 active area, 500 µm thickness, placed 3 mm above the sample.
- **XRR detector:** PIXcel3D (Medipix2) detector used in open detector (0D) mode.

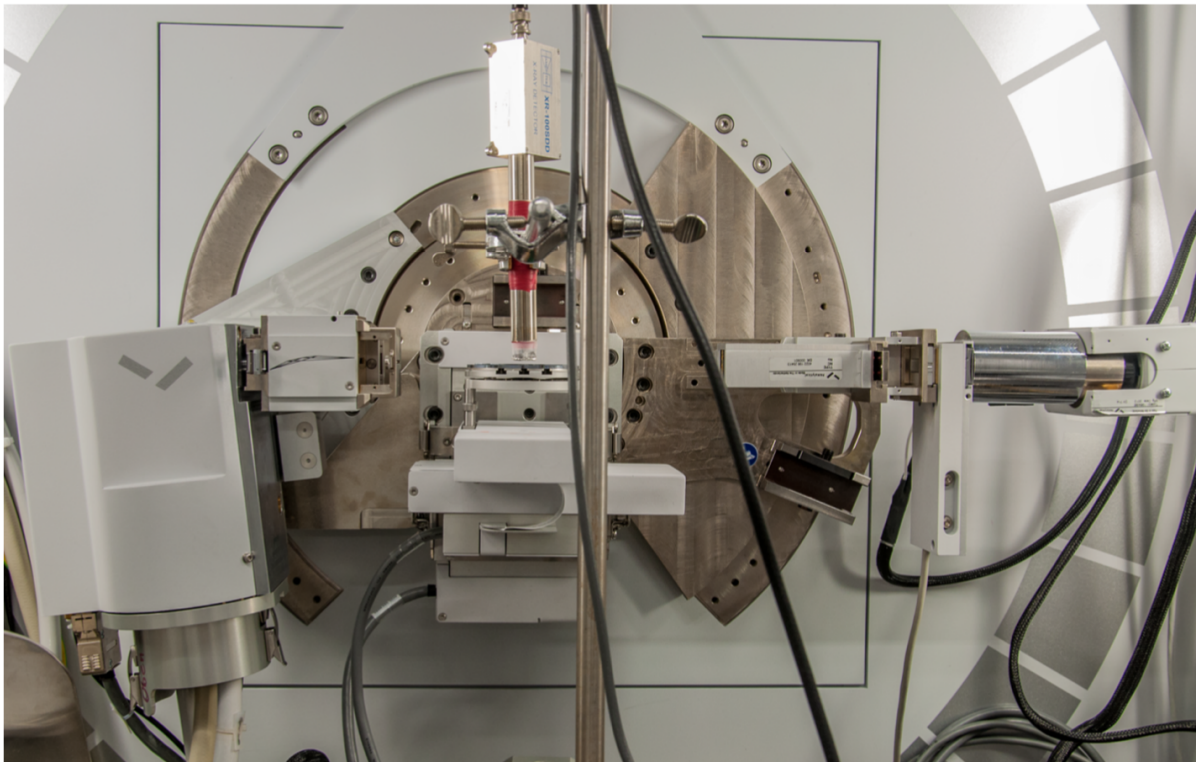

Figure 31: Setup at the XRC from [7]

The setup parameter are shown in table 3.

Variated	Parameter	Minimum	Start	Maximum
	Shape		gaussian	
	Beam height (µm)		80.0	
✓	**Divergence** (mrad)	0.1	0.3	0.5
	Photon energy (eV)		8047.8 (Cu-KL3)	
	Detector angle (deg)		90.0	
✓	**Visible length** (mm)	3.0	6.0	9.0
✓	**Divergence** (mrad)	0.1	0.2	0.3
✓	**Si-KL3**	0.0	1.0	10^{20}
✓	**XRR**	0.0	1.0	10^{20}
	Sample rotating		false	

Table 3: Setup for the measurement 20160310_Ni50-00031a (XRC)

Table 4 shows the results for the variated parameters.

Parameter	jGiXa 1.0	jGiXa 2.0	Deviation of jGiXa 2.0 from jGiXa 1.0 (%)
X-ray-Source **Divergence (mrad)**	0.195	0.201	2.87
XRF-Detector **Visible length (mm)**	8.207	8.238	0.38
XRR-Detector **Divergence (mrad)**	0.129	0.131	1.75
Si-KL3-Sensitivity	$1.128E8$	$1.126E8$	0.15
XRR-Sensitivity	$1.623E7$	$1.621E7$	0.11
Sample length (mm)	168.588	191.601	13.66
NiO_2 **Thickness (nm)**	3.759	3.761	0.07
Density (g/cm^3)	1.880	1.874	0.32
Roughness (nm)	0.810	0.808	0.34
Ni **Thickness (nm)**	52.976	52.962	0.03
Density (g/cm^3)	8.904	8.917	0.15
Roughness (nm)	1.229	1.230	0.11
Si (Substrate) **Roughness (nm)**	0.344	0.344	0.14

Table 4: Comparison of results for the measurement 20160310_Ni50-00031a (XRC) evaluated with jGiXa 1.0 and jGiXa 2.0

Figure 32 shows the calculated and measured curves of the different X-ray lines.

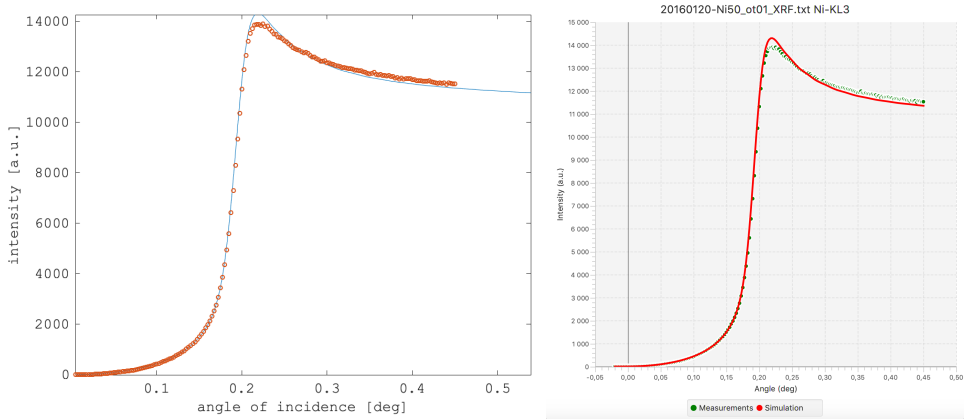

(a) Ni-KL3: jGiXa 1.0 (left), jGiXa 2.0 (right)

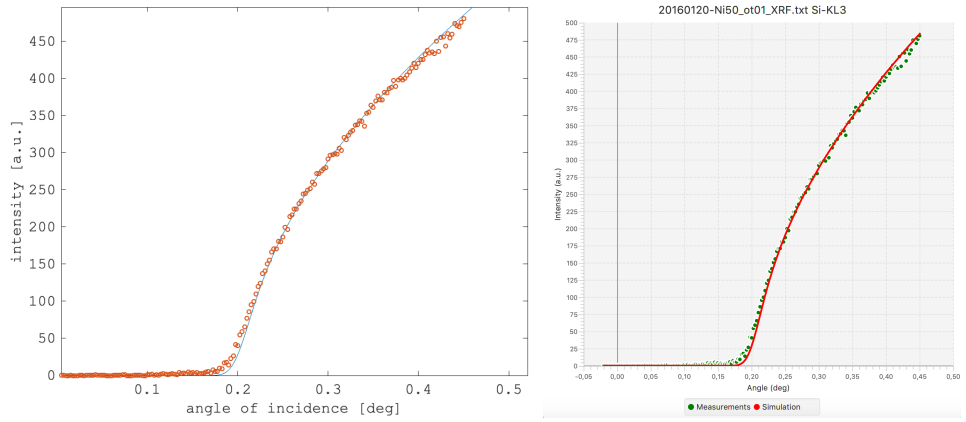

(b) Si-KL3: jGiXa 1.0 (left), jGiXa 2.0 (right)

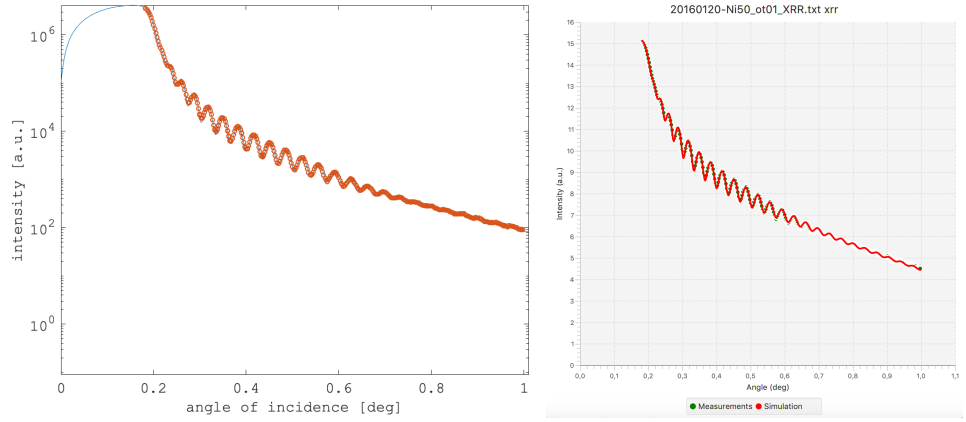

(c) XRR: jGiXa 1.0 (left), jGiXa 2.0 (right)

Figure 32: Plots of calculated and measured curves of the measurement 20160310_Ni50-00031a (XRC)

The results fit very well with deviations of 3% or less, except for the sample length with 14 %. Investigations concerning the sample length showed, that variations of the sample length for sample lengths larger than 100 mm don't affect the result in a noticeable way (see figure 28). Especially the parameters for the sample model of the layers, which can be considered as the main subject of the investigation, fit very well with deviations smaller than 1% and layer thickness deviations even smaller than 1 ‰.

4.1.2 Measurement from the Atominstitut (ATI) of the TU Wien

The measurement 20160120-Ni50_ot01 was taken at the Atominstitut (ATI) of the TU Wien, using the following setup:

- **X-ray source:** 2kW Siemens FF 0.4×8 mm (fine focus) Molybdenum, exit window 300 μm beryllium
- **Monochromator:** multilayer from a commercial TXRF wafer analyzer (Atomika 8010 W)
- **XRF detector:** Vortex-60EX with Be entrance window, 50 mm^2 active area, 350 µm thickness
- **XRR detector:** Amptek AXR PA-230 PX5 with Be entrance window, 25 mm^2 active area, 500 µm thickness

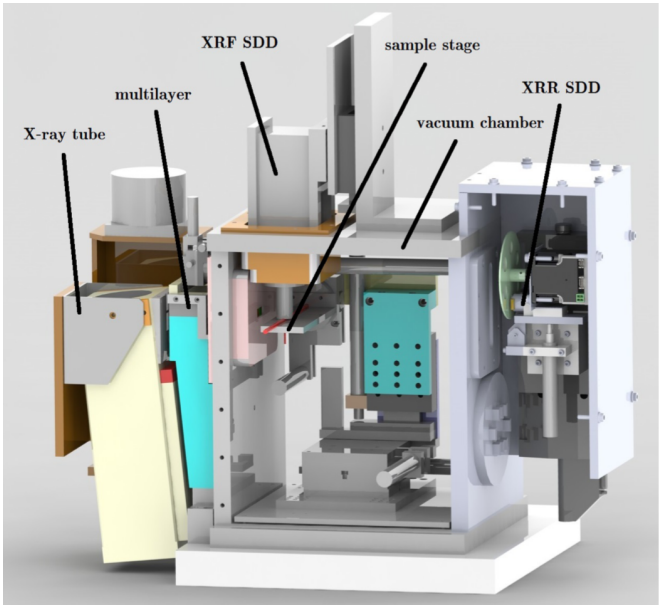

Figure 33: Setup at the ATI from [7]

The setup parameter are shown in table 5.

Variated	Parameter	Minimum	Start	Maximum
	Shape		gaussian	
	Beam height (µm)		50.0	
✓	**Divergence** (mrad)		0.4	
	Photon energy (eV)		17478.0 (Mo-KL3)	
	Detector angle (deg)		90.0	
✓	**Visible length** (mm)		2.0	
✓	**Divergence** (mrad)		0.23	
✓	**Si-KL3**	0.0	1.0	10^{20}
✓	**XRR**	0.0	1.0	10^{20}
	Sample rotating		false	

Table 5: Setup for the measurement 20160120-Ni50_ot01 (ATI)

Table 6 shows the results for the variated parameters.

Parameter	jGiXa 1.0	jGiXa 2.0	Deviation of jGiXa 2.0 from jGiXa 1.0 (%)
Si-KL3-Sensitivity	$4.427E6$	$4.400E6$	0.15
Ni-KL3-Sensitivity	$2.248E9$	$2.252E9$	0.15
XRR-Sensitivity	X	$5.105E6$	0.11
Sample length (mm)	25.782	28.776	13.66
NiO_2 **Thickness (nm)**	3.566	3.559	0.07
Density (g/cm^3)	1.404	1.240	0.32
Roughness (nm)	0.783	0.715	0.34
Ni **Thickness (nm)**	52.656	52.599	0.03
Density (g/cm^3)	8.751	8.741	0.15
Roughness (nm)	1.354	1.358	0.11
Si (Substrate) **Roughness (nm)**	0.300	0.296	0.14

Table 6: Comparison of results for the measurement 20160120-Ni50_ot01 (ATI) evaluated with jGiXa 1.0 and jGiXa 2.0

Figure 34 shows the calculated and measured curves of the different X-ray lines.

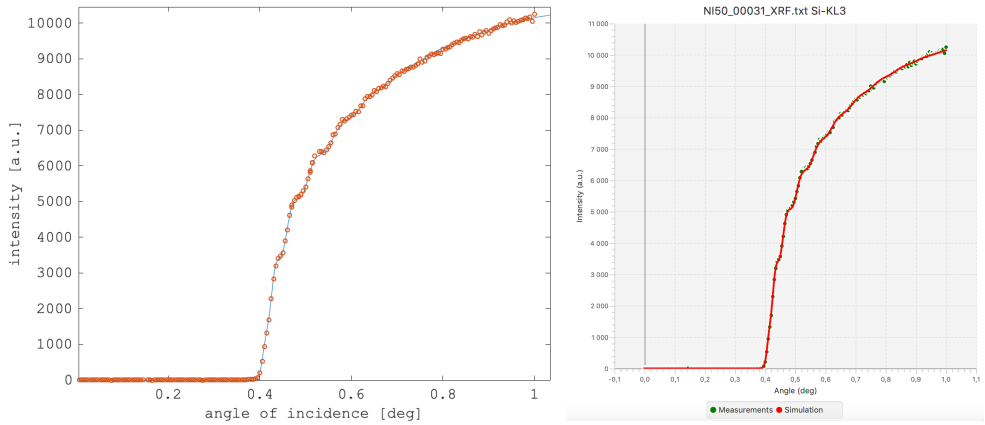

(a) Si-KL3: jGiXa 1.0 (left), jGiXa 2.0 (right)

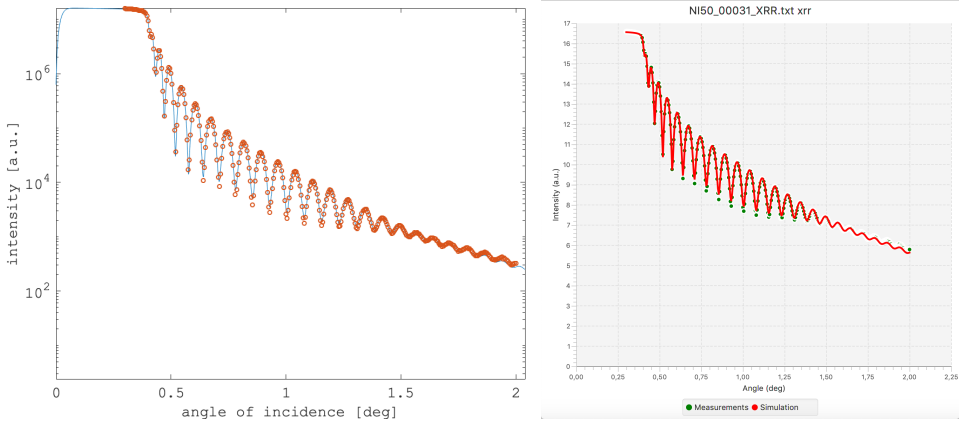

(b) XRR: jGiXa 1.0 (left), jGiXa 2.0 (right)

Figure 34: Plots of calculated and measured curves of the measurement 20160120-Ni50_ot01 (ATI)

Again the results are very satisfactory, with deviations for the sample model parameter smaller than 1% and deviations for the layer thickness smaller than 1 ‰. The 14 % deviation of the sample length parameter is negligible since it doesn't noticeably affect the resulting curve (see figure 28).

4.2 Evaluation of a Ti sample with jGiXa 2.0

To test the new model for intermediate layers, two measurements of different Ti samples were evaluated with a new sample model, including intermediate layers. The initial models of the sample were a Ti layer, with a thickness of 10 / 18 nm respectively on a thick SiO_2 layer. On top of the Ti layer two TiO_2 layers with different densities were added to consider possible oxidation processes.

4.2.1 Ti sample with a nominal thickness of 10 nm

The measurement 201804_D385-00001-cps-01-01pa was taken at the X-Ray Center (XRC) of the TU Wien, with the setup from section 4.1.1. The results of the different sample models are shown in table 7 and the corresponding plots in figure 35.

Layer	Parameter	jGiXa 1.0	jGiXa 2.0	jGiXa 2.0 Intermediate Layer	
TiO_2	Thickness (nm)	1.51	0.92	0.10	0.76
	Density (g/cm^3)	0.67	3.16	3.17	
	Roughness (nm)	0.12	0.96	0.96	
Intermediate	Thickness (nm)			1.31	
	Steps			5	
	$T_{Composition}$			0.05	
	$T_{Density}$			0.13	
TiO_2	Thickness (nm)	4.96	4.90	2.18	4.69
	Density (g/cm^3)	4.03	4.07	4.02	
	Roughness (nm)	0.63	0.18	0.0	
Intermediate	Thickness (nm)			3.70	
	Steps			5	
	$T_{Composition}$			0.30	
	$T_{Density}$			0.16	
Ti	Thickness (nm)	9.40	9.17	6.40	9.37
	Density (g/cm^3)	4.56	4.46	4.53	
	Roughness (nm)	0.38	0.41	0.0	
Intermediate	Thickness (nm)			2.24	
	Steps			5	
	$T_{Composition}$			0.39	
	$T_{Density}$			0.18	
SiO_2	Thickness (nm)	300.0	300.0	300.0	
	Density (g/cm^3)	2.2	2.2	2.2	
	Roughness (nm)	0.28	0.28	0.0	
Si	Thickness (nm)	∞	∞	∞	
	Density (g/cm^3)	2.33	2.33	2.33	
	Roughness (nm)	0.30	0.30	0.30	
Best χ^2		0.0019	0.0042	0.0040	

Table 7: Comparison of results of the measurement 201804_D385-00001-cps-01-01pa (10 nm) without intermediate layer with jGiXa 1.0 (left), with jGiXa 2.0 (middle) and with intermediate layer with jGiXa 2.0 (right). The parameters in the cells marked in gray have not been variated. The colored numbers show a comparable thickness of the layers, calculated by adding half the thickness of the neighbouring intermediate layers (colored cells) to the layer thickness.

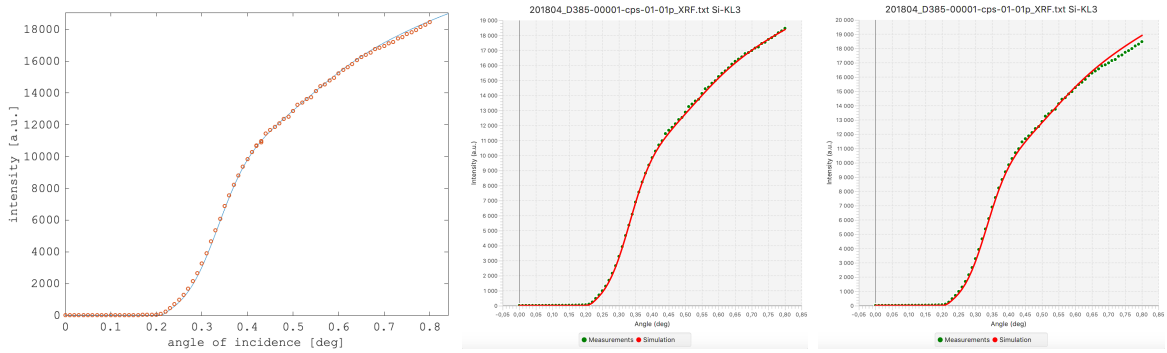

(a) Si-KL3: jGiXa 1.0 (left), jGiXa 2.0 (middle), jGiXa 2.0 with intermediate layer model(right)

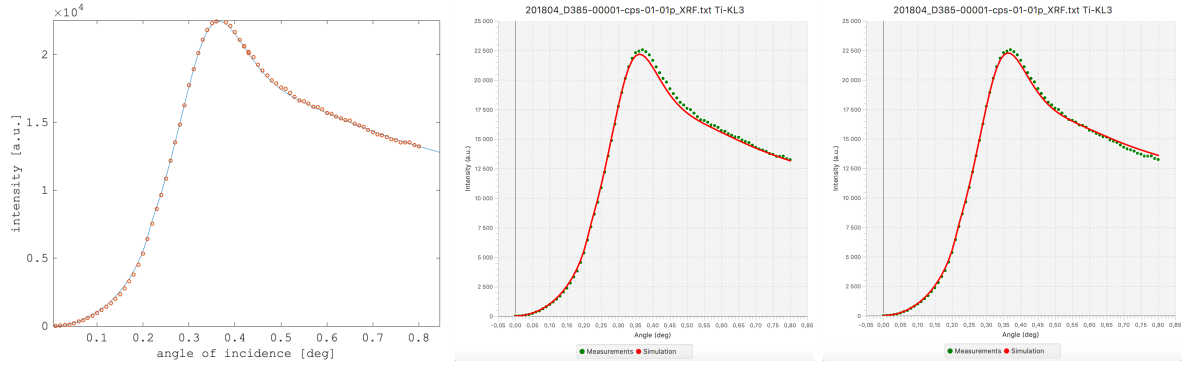

(b) Ti-KL3: jGiXa 1.0 (left), jGiXa 2.0 (middle), jGiXa 2.0 with intermediate layer model(right)

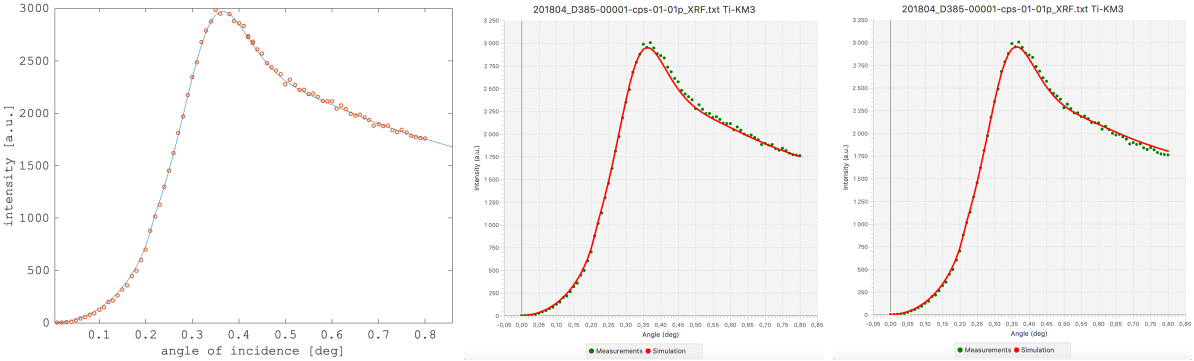

(c) Ti-KM3: jGiXa 1.0 (left), jGiXa 2.0 (middle), jGiXa 2.0 with intermediate layer model(right)

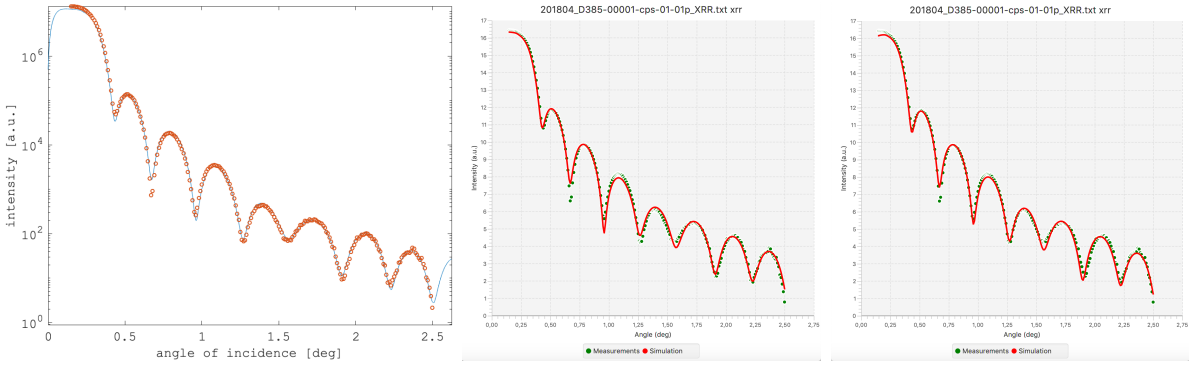

(d) XRR: jGiXa 1.0 (left), jGiXa 2.0 (middle), jGiXa 2.0 with intermediate layer model(right)

Figure 35: Plots of calculated and measured curves of the measurement 201804_D385-00001-cps-01-01pa (10 nm)

4.2.2 Ti sample with a nominal thickness of 18 nm

The measurement 201804_D389-00003-cps-01p was taken at the X-Ray Center (XRC) of the TU Wien, with the setup from section 4.1.1. The results of the different sample models are shown in table 8 and the corresponding plots in figure 36.

Layer	Parameter	jGiXa 1.0	jGiXa 2.0	jGiXa 2.0 Intermediate Layer	
TiO_2	Thickness (nm)	1.54	0.64	0.47	0.92
	Density (g/cm^3)	0.65	3.30	3.3	
	Roughness (nm)	0.30	1.00	0.92	
Intermediate	Thickness (nm)			0.89	
	Steps			5	
	$T_{Composition}$			0.20	
	$T_{Density}$			0.25	
TiO_2	Thickness (nm)	4.73	4.70	2.55	4.83
	Density (g/cm^3)	3.92	4.09	4.2	
	Roughness (nm)	0.67	0.30	0.0	
Intermediate	Thickness (nm)			3.67	
	Steps			5	
	$T_{Composition}$			0.18	
	$T_{Density}$			0.08	
Ti	Thickness (nm)	18.42	18.19	15.60	18.02
	Density (g/cm^3)	4.46	4.46	4.45	
	Roughness (nm)	0.55	0.40	0.0	
Intermediate	Thickness (nm)			1.17	
	Steps			5	
	$T_{Composition}$			0.02	
	$T_{Density}$			0.24	
SiO_2	Thickness (nm)	300.0	300.0	300.0	
	Density (g/cm^3)	2.2	2.2	2.2	
	Roughness (nm)	0.25	0.27	0.0	
Si	Thickness (nm)	∞	∞	∞	
	Density (g/cm^3)	2.33	2.33	2.33	
	Roughness (nm)	0.30	0.30	0.30	
Best χ^2		0.0019	0.0021	0.0026	

Table 8: Comparison of results of the measurement 201804_D389-00003-cps-01p (18 nm) without intermediate layer with jGiXa 1.0 (left), with jGiXa 2.0 (middle) and with intermediate layer with jGiXa 2.0 (right). The parameters in the cells marked in gray have not been variated. The colored numbers show a comparable thickness of the layers, calculated by adding half the thickness of the neighbouring intermediate layers (colored cells) to the layer thickness.

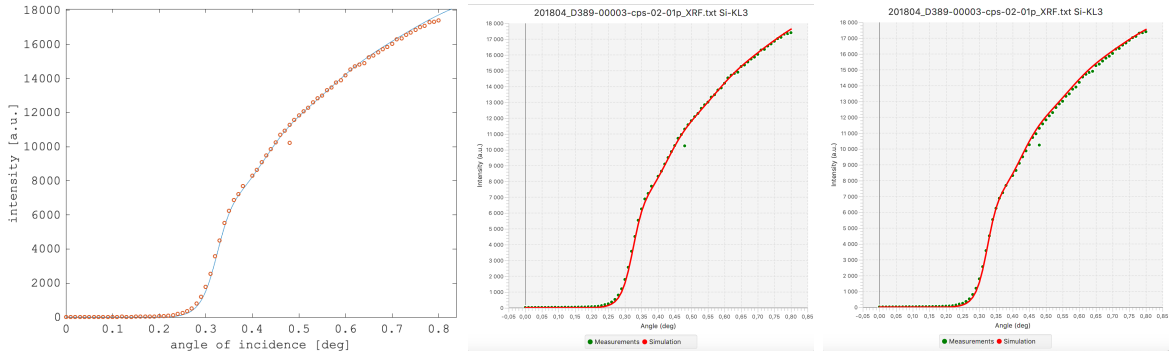

(a) Si-KL3: jGiXa 1.0 (left), jGiXa 2.0 (middle), jGiXa 2.0 with intermediate layer model(right)

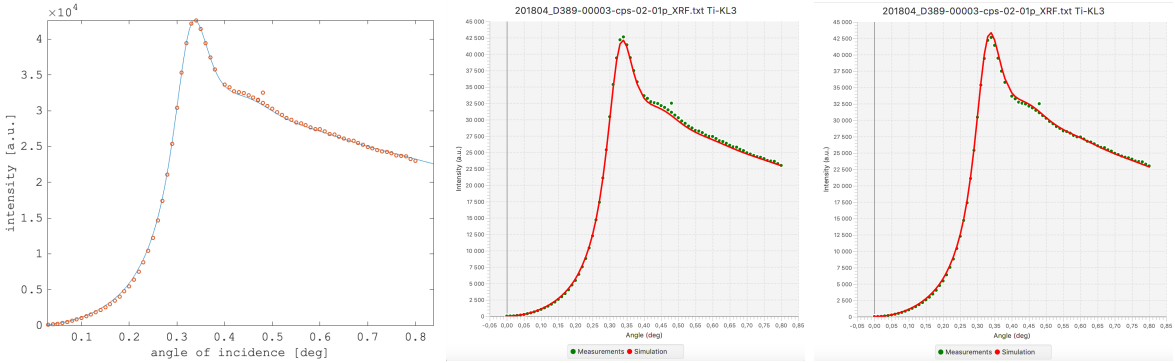

(b) Ti-KL3: jGiXa 1.0 (left), jGiXa 2.0 (middle), jGiXa 2.0 with intermediate layer model(right)

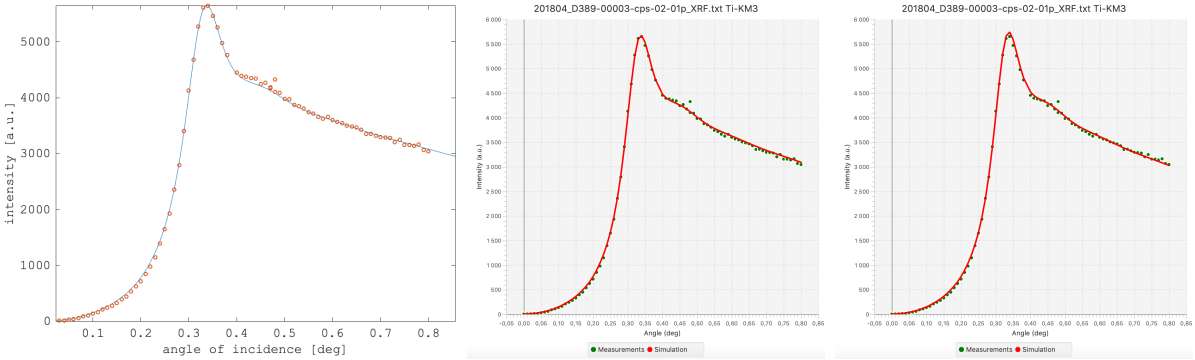

(c) Ti-KM3: jGiXa 1.0 (left), jGiXa 2.0 (middle), jGiXa 2.0 with intermediate layer model(right)

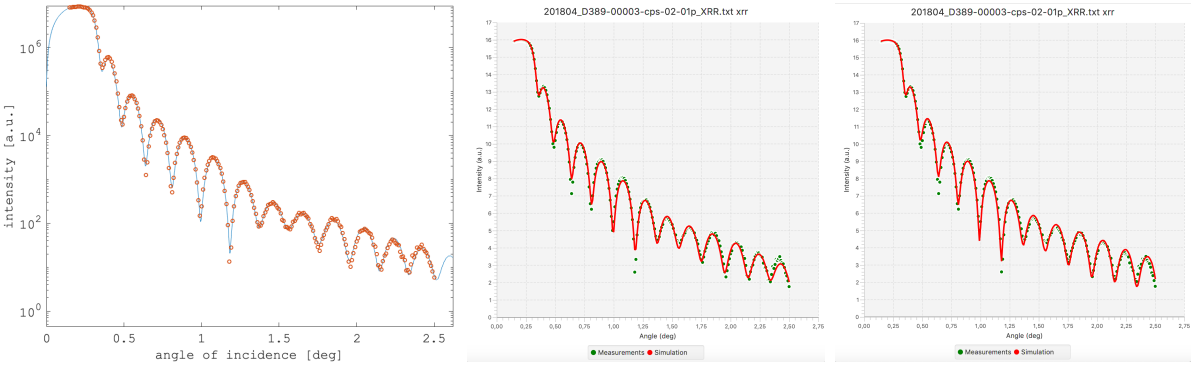

(d) XRR: jGiXa 1.0 (left), jGiXa 2.0 (middle), jGiXa 2.0 with intermediate layer model(right)

Figure 36: Plots of calculated and measured curves of the measurement 201804_D389-00003-cps-01p (18 nm)

The evaluations with the new model, result in solutions of similar quality, i.e. weighted χ^2, as the evaluations with the sample model without intermediate layers. As also discussed in section 4.3 direct comparisons to the χ^2 of jGiXa 1.0 can not be made, due to slight changes in the calculation of χ^2, but solutions with χ^2 in the same order of magnitude are satisfactory, making the new model a success for the investigation of intermediate layers. To visualize comparable results for layer thicknesses tables 7 & 8 show (in green color) comparable main layer thicknesses with deviations of less than 3 %, calculated by adding half of the thickness of the upper and lower intermediate layer to the layer thickness. The vastly higher calculation time and the high sensitivity of the convergence towards a correctly chosen sample model make it recommendable to use sample models with intermediate layers only if the transition layers are of explicit interest and after a previous investigation of the layers of the sample model with the single parameter roughness model. For those investigations the optimization can be used to get information about the transition function and thickness of the intermediate layer (see section 3.6), thus expanding the functionality of jGiXa.

4.3 Performance

To compare the performance of jGiXa 2.0 with its predecessor, the evaluations from section 4.1.1, performed on a PC with an Intel(R) Core(TM) i7-6850K CPU (3.6GHz, 12CPUs) and 16 GB RAM, where timed. The optimizations ran for 2000 iteration steps, which proved to be a sufficiently large number to guarantee a global minimum, of the problem (see section 4.1.1). The comparison of speed is shown in table 9.

	Time (s)	**Final χ^2**
jGiXa 1.0	7223,4	$3.9 \cdot 10^{-4}$
jGiXa 2.0	1074,7	$4.3 \cdot 10^{-4}$

Table 9: Evaluation time and minimum χ^2 for 2000 iteration of the problem from section 4.1.1

Taking the matching results (see section 4.1.1) into account, the roughly 10% difference of the weighted χ^2 values can be considered negligible. Also slight variations of χ^2 are expected due to a different weighting of the χ^2 values, for jGiXa 1.0 and jGiXa 2.0. The improvement of speed of roughly a factor 7 is in the case of this rather simple sample model, equivalent to an improvement from roughly 2 hours per optimization to roughly 20 minutes per optimization.

4.4 Meta optimization

The differential evolution algorithm [8, 9] is a powerful global optimization algorithm applicable to various problems. The algorithm itself has many parameters that can be variated. Before discussing this optimization of the parameters of the algorithm, i.e. the meta optimization, a short explanation of the functional principle of the algorithm, based on the optimizations performed by jGiXa, should be given here.

4.4.1 Differential evolution

The aim of the differential evolution algorithm implemented in jGiXa is to find the values of a chosen set of variation parameters p_1, p_2, p_3, ... (e.g. Visible sample length, Angular divergence, Thickness of a layer,...), for which the the weighted χ^2 function $\chi^2(p_1, p_2, p_3, ...)$ reaches a minimum. In the following the parameter set will be represented by the solution vector $\vec{p} = (p_1, p_2, p_3, ...)$, with the dimension of the solution vector being the number of parameters chosen for variation. The function $\chi^2(\vec{p})$ represents the summed up deviation of the simulated curves to the measured curves, i.e. the quality of the solution, with small values of χ^2 for good solutions. The aim of the algorithm is to find the global minimum of the function $\chi^2(\vec{p})$, i.e. the best solution vector. Before discussing them and the algorithm in more detail a list of the parameters for the algorithm, chosen by the user is given here:

- **Population size** N_P is the number of solution vectors generated each iteration step.
- **Step size** F is a factor used in the calculation of a new solution vector entry as a linear combination of old solution vector entries.
- **Crossover probability** Cr is a factor determining the probability of calculating a new solution vector entry in each iteration step.
- **Strategy** St is the specific rule how new solution vector entries are calculated.
- **Boundary Constraints** B is a rule how the optimization handles calculated values outside the user specified boundary constraints, i.e. maximum and minimum of a parameter p_i.
- **Value to reach** V determines the value of χ^2 for which the optimization can be stopped.

- **Maximum number of iterations** I_{max} determines the maximum number of iteration steps if χ^2 does not reach V.

At first the optimization creates N_P solution vectors $\vec{p}^1, \vec{p}^2, \vec{p}^3, ..., \vec{p}^{N_P}$, with entries randomly generated between the user determined boundaries of each parameter, and calculates their $\chi^2(\vec{p})$. In every following iteration step a random number between 0 and 1 is generated for each entry of each solution vector. If the generated number is smaller than the crossover probability Cr, the entry of the according vector in this iteration step is changed to a value calculated through linear combination of the same entries of different vectors of the previous iteration step, using the step size F. To get an idea how these strategies work three strategies are explained in more detail. In the following the i-th entry of the n-th solution vector of the previous generation is written as p_i^n and the according entry of the new generation is written as q_i^n. Thus p_i^{best} is the i-th entry of the solution vector of the previous generation with the best χ^2 and $p_i^{rand_1}$, $p_i^{rand_2}$ and $p_i^{rand_3}$ are the i-th entries of random solution vectors of the previous generation.

- **best1bin** calculates $q_i^n = p_i^{best} + F \cdot (p_i^{rand_1} - p_i^{rand_2})$
- **rand1bin** calculates $q_i^n = p_i^{rand_1} + F \cdot (p_i^{rand_2} - p_i^{rand_3})$
- **current2rand** calculates $q_i^n = p_i^n + Cr \cdot (p_i^{rand_1} - p_i^n) + F \cdot (p_i^{rand_2} - p_i^{rand_3})$

with all **best**-strategies using the initial vector entry p_i^{best}, all **rand**-strategies using the initial vector entry p_i^{rand} and all **current**-strategies using the initial vector entry p_i^n to calculate the new vector entry q_i^n. This process can create values outside the user determined boundary constraints and lead to results with no sensible physical interpretation, e.g. negative layer thickness. To consider the boundary constraints of each optimization parameter, different ways of handling generated values outside the constraints can be used. In the following the user determined boundary constraints of the i-th parameter are written as min_i and max_i, q_i^n is the value for the i-th entry of the n-th vector initially calculated by the strategy, $q_i^{n\prime}$ is the entry of the final vector and p_i^{start} is the i-th entry of the initially used vector to calculate q_i^n (depending on the strategy p_i^{best}, p_i^{rand} or p_i^n, see above) and r being a random number between 0 and 1.

- **bounceBack** calculates
  $q_i^{n\prime} = p_i^{start} + (max_i - p_i^{start}) \cdot r$ if $q_i^n > max_i$ or
  $q_i^{n\prime} = min_i + (p_i^{start} - min_i) \cdot r$ if $q_i^n < min_i$ or otherwise
  $q_i^{n\prime} = q_i^n$

- **randReInit** calculates
  $q_i^{n\prime} = (max_i - min_i) \cdot r$ if $q_i^n < min_i$ or $q_i^n > max_i$ or otherwise
  $q_i^{n\prime} = q_i^n$

- **discardNew** calculates
  $q_i^{n\prime} = p_i^n$ if $q_i^n < min_i$ or $q_i^n > max_i$ or otherwise
  $q_i^{n\prime} = q_i^n$

After the new generation of solution vectors are calculated, each $\chi^2(\vec{q}^n)$ is compared with $\chi^2(\vec{p}^n)$ keeping only the vector with the better, i.e. smaller, χ^2 as a vector of the old generation for the next iteration step. A more detailed explanation of the algorithm can be found in [8, 9].

4.4.2 Investigation of a possible best parameter set

To investigate the possible existence of an ideal parameter set for GIXA in general or of a subset of problems, with a similar setup-sample-model, a meta-optimization was conducted, varying the following parameters, for the problem from section 4.1.1:

- **Step size** F: 0.5, 0.6, 0.7, 0.8, 0.9, 1.0
- **Crossover probability** Cr: 0.1, 0.2, 0.8, 0.9
- **Strategy** St: best1bin, best1exp, best2bin, best2exp, best3bin, current2rand, rand1bin, rand2bin, rand1exp, rand2exp, randToBest1Bin, randToBest1Exp, randRandBin
- **Boundary Constraints** B: bounceBack, randReInit, discardNew

The varied parameter combine to 936 different optimization problems. This brute-force method to test the different parameter sets could be done in a reasonable time (roughly one week, using the computer from section 4.3) due to the vast improvement of speed from jGiXa 1.0 to jGiXa 2.0 (see section 4.3). The range of the step size was chosen, because literature suggests that step sizes smaller than 0.5 or larger than 1.0 are somewhat exotic (see [8, 9]). Also it is recommended to use either small or large crossover probabilities, because crossover probabilities of around 0.5 don't seem to converge well. An ideal set of parameter is a set that guarantees the convergence against the global minimum of the χ^2 function, and converges as fast as possible. To find a parameter set like this the influence of different setup combinations on the convergence behavior was investigated.

Averaging all optimizations of the same strategy leads to an interesting result. The two standard strategies best1bin and rand1bin are on long term converging against the worst and the best on average weighted χ^2 of all possible strategies. This of course does not mean that there are no parameter combinations where best1bin or other strategies find the global minimum, sometimes they even converge faster, but in general it seems that the safest strategy to find the global minimum with almost all combinations of parameters seems to be rand1bin. Figure 37 shows the progression of χ^2 over the iteration steps for the different investigated strategies.

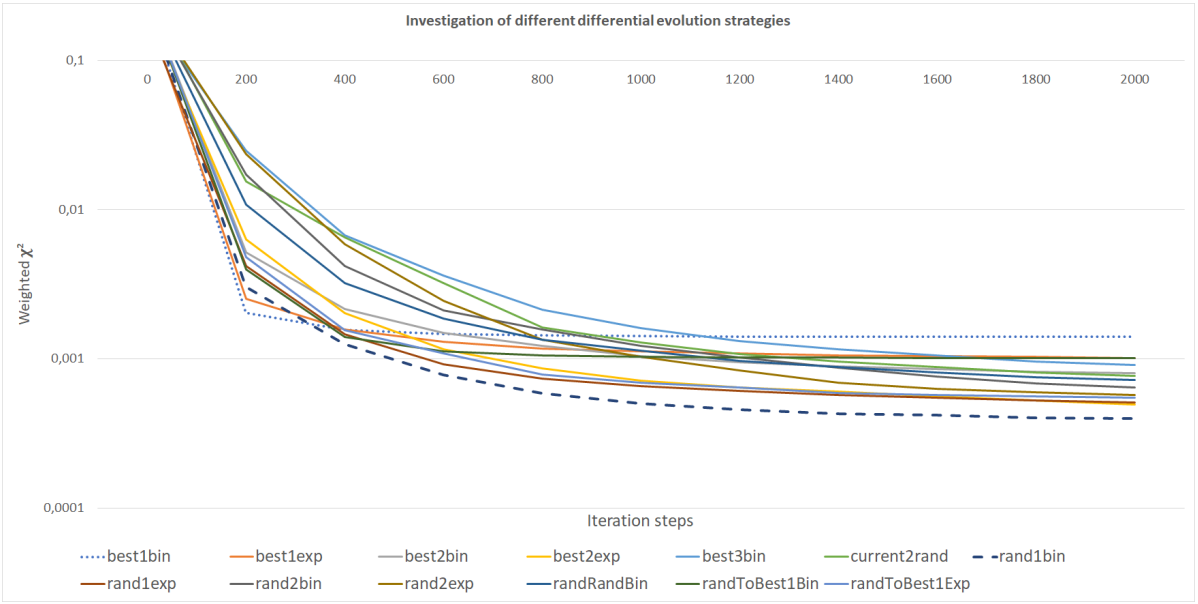

Figure 37: Convergence for different strategies

The averaged convergence for the different boundary conditions in general (see figure 38) shows, that the bounceBack boundary constraints seem to converge fast in the beginning but in some cases seem not to find the global minimum. The safest boundary constraints in general therefore are randReInit and discardNew, with randReinit generally being the faster one.

Further investigating only the rand1bin strategy, to find the ideal parameter set, seems to show a faster convergence for combinations with small F and large Cr. This is shown in figure 39.

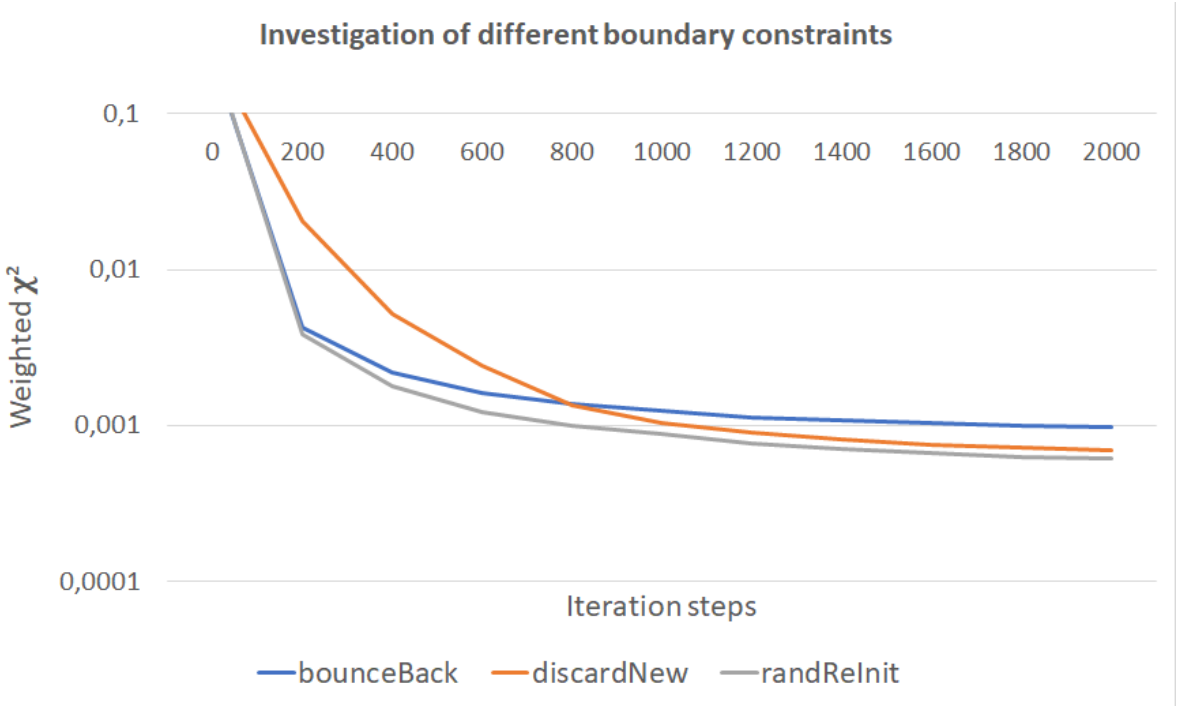

Figure 38: Convergence for different boundary conditions

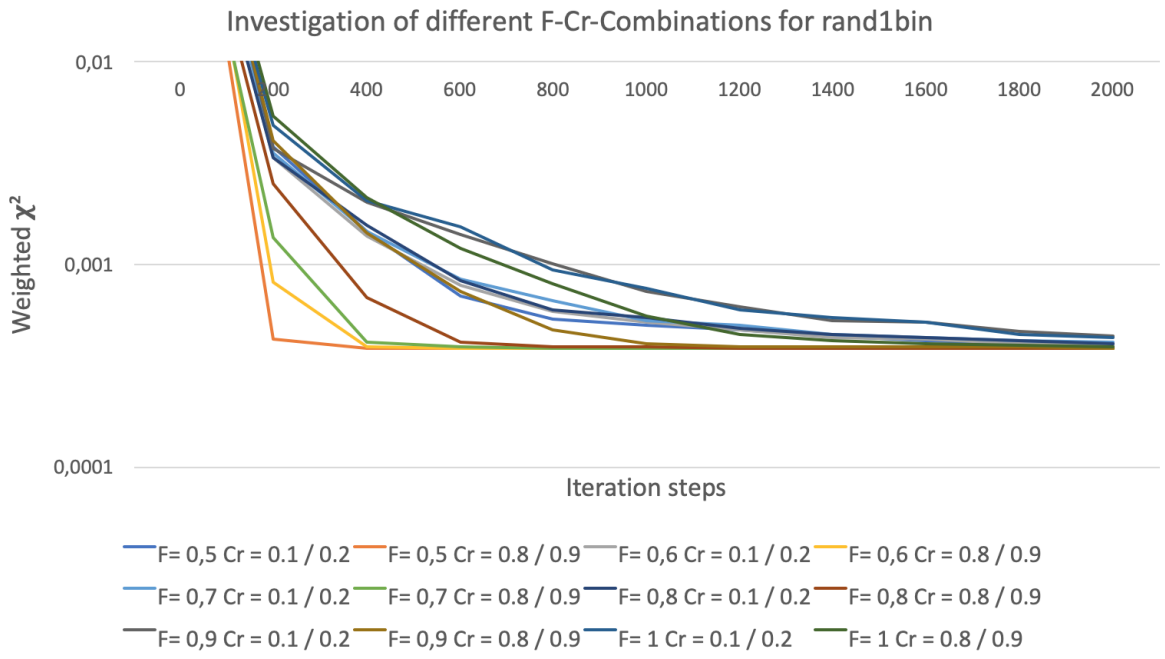

Figure 39: Convergence for different boundary conditions

The recommended optimization, to make certain the best solution is found and optimize the speed of the optimization after investigation, is therefore:

- **Step size** F: 0.5 / 0.6
- **Crossover probability** Cr: 0.8 / 0.9
- **Strategy:** rand1bin
- **Boundary Constraints:** randReInit

5 Conclusions and Outlook

The further development of jGiXa, was tested to be highly successful in respect to speed and functionality. Comparison evaluations between jGiXa 1.0 and its successor, showed a vast improvement of speed, for results of equal quality. The newly implemented roughness model using intermediate layers was also successfully tested, making it possible to investigate samples with continuous transitions between materials. The meta optimization of the implemented differential evolution algorithm makes it possible to use jGiXa with a parameter set optimized for accuracy and performance. To further investigate possible deviations from the result of the meta optimization the meta optimization should be applied to various evaluations with different sample models in the future. The new structure of the project makes jGiXa a more easy to setup, easy to use and easy to maintain, platform independent software package, applicable to different experimental setups. Further development can be divided in to small sub-tasks more easily, because new developers can get a quicker clear overview of the different parts of jGiXa and don't need to be proficient in both Java and MatLab syntax. A list of ideas for possible features is given here for future developers, i.e. project students, working on jGiXa:

- Advanced plotting functions, allowing to create and manipulate more sophisticated plots.
- Advanced meta optimization functions, allowing to perform the meta optimization on a stop and go basis.
- More global optimization algorithms (Particle Swarm Optimization, Levenberg-Marquardt algorithm)
- Functions to import and manipulate the measured spectra directly
- Functions to apply multiple setups, with according measurements to one sample model in the same optimization.
- Functions to perform calculations for polychromatic primary radiation

References

[1] W. Van Den Hoogenhof and D. de Boer. "Glancing incidence X-ray analysis". In: *Spectrochimica Acta* 48B.2 (1993).

[2] D. Ingerle et al. "JGIXA: A software package for the calculation and fitting of grazing incidence X-ray fluorescence and X-ray reflectivity data for the characterization of nanometer-layers and ultra-shallow-implants". In: *Spectrochimica Acta Part B* (2016).

[3] D. de Boer, A. J. G. Leenaers, and W. Van Den Hoogenhof. "The Profile of Layered Materials Reflected by Glancing-Incidence X-Ray Analysis". In: *Applied Physics A* 58 (1994).

[4] D. de Boer and W. Van Den Hoogenhof. "Glancing Incidence X-ray Analysis: Forgotten or to be Discovered?" In: *Surface and Interface analysis* 22 (1994).

[5] D. de Boer. "Glancing incidence X-ray fluorescence of layered materials". In: *Physical Review B* 44.2 (1991).

[6] D. de Boer, A. J. G. Leenaers, and W. Van Den Hoogenhof. "Glancing incidence X-ray analysis of Thin-Layered Materials: a Review". In: *X-ray spectrometry* 24 (1995).

[7] D.Ingerle. "Grazing incidence X-ray fluorescence combined with X-ray reflectivity: development of an evaluation software". PhD thesis. Technische Universität Wien, 2017.

[8] K. Price, R. Storn, and J. Lampinen. *Differential Evolution: A Practical Approach to Global Optimization*. Springer-Verlag Berlin Heidelberg, 2005.

[9] K. Price and R. Storn. *http://www1.icsi.berkeley.edu/~storn/code.html*. (Visited on 04/18/2019).

[10] E. Gamma et al. *Design Patterns: Elements of Reusable Object-Oriented Software*. Addison-Wesley, 1994.

[11] R. van Grieken and A. Markowicz. *Handbook of X-ray Spectrometry*. 2nd ed. Marcel Dekker, Inc., 2002.

[12] W. Demtröder. *Experimentalphysik 3*. 4th ed. Springer-Verlag Berlin Heidelberg, 2010.

[13] R. Klockenkämper and A. von Bohlen. *Total-Reflection X-Ray Fluorescence Analysis and Related Methods*. John Wiley and Sons, Inc., 2014.

[14] J. Als-Nielsen and D. McMorrow. *Elements of Modern X-ray Physics*. John Wiley and Sons, Inc., 2011.

[15] Public domain. *https://commons.wikimedia.org/wiki/File:BraggPlaneDiffraction.svg*. (Visited on 04/18/2019).

[16] C. T. Chantler. "Detailed tabulation of atomic form factors, photoelectric absorption and scattering cross section, and mass attenuation coefficients in the vicinity of absorption edges in the soft X-ray (Z = 30-36, Z = 60-89, E = 0.1-10 keV)". In: *Journal of Synchrotron Radiation* (2001).

[17] H. Breuer. *dtv-Atlas zur Physik Band 1*. 51996th ed. Deutscher Taschenbuch Verlag GmbH & Co. KG, 1996.

[18] Oxford Instruments. *https://www.exvil.lt/wp-content/uploads/2012/04/SDD_Explained.pdf*. (Visited on 04/18/2019).

[19] H. Schwenke, J. Knoth, and U. Weisbrod. "Current work on total reflection x-ray fluorescence spectrometry at the GKSS research centre". In: *X-Ray Spectrometry* (1991).

[20] P. Croce and L. Névot. "Étude des couches minces et des surfaces par réflexion rasante, spéculaire ou diffuse, de rayons X". In: *Revue de Physique Appliquée* (1976).

[21] K. Stoev and K. Sakurai. "Recent theoretical models in Grazing incidence X-ray reflectometry". In: *The Rigaku Journal* 14.2 (1997).

[22] B. Großmayer. "Softwarepaket zur quantitativen Röntgenfluoreszenzanalyse mittels fundamentaler Parameter unter Verwendung von Röntgenoptiken". MA thesis. Technische Universität Wien, 2009.

[23] D. de Boer. "X-ray scattering and x-ray fluorescence from materials with rough interfaces". In: *Physical Review B* 53.10 (1996).

[24] D. de Boer and W. Van Den Hoogenhof. "Total reflection X-ray fluorescence of single and multiple thin-layer samples". In: *Spectrochimica Acta* 46B.10 (1991).

[25] D. de Boer. "X-ray Standing Waves and the critical sample thickness for Total-reflexion X-Ray Fluorescence analysis". In: *Spectrochimica Acta* 46B.10 (1991).

[26] D. Ingerle. "A new spectrometer for grazing incidence X-ray fluorescence for the characterization of Arsenic implants and Hf based high- κ-layers". MA thesis. Technische Universität Wien, 2015.

[27] D. Ingerle et al. "Combination of grazing incidence x-ray fluorescence with x-ray reflectivity in one table- top spectrometer for improved characterization of thin layer and implants on/in silicon wafers". In: *Review of scientific instruments* (2014).

[28] D. Ingerle et al. "Combined evaluation of grazing incidence X-ray fluorescence and X-ray reflectivity data for improved profiling of ultra-shallow depth distributions". In: *Spectrochimica Acta Part B* (2014).

[29] F. Brigidi and G. Pepponi. "GIMPy: a software for the simulation of X-ray fluorescence and reflectivity of layered materials". In: *X-ray spectrometry* (2016).

[30] M. K. Tiwari, G. S. Lodhab, and K. J. S. Sawhney. "Applications of the CATGIXRF computer program to the grazing incidence X-ray fluorescence and X-ray reflectivity characterization of thin films and surfaces". In: *X-ray spectrometry* (2009).